LANGMUIR

pubs.acs.org/Langmuir

Invited Feature Article

Design and Preparation of Nematic Colloidal Particles

Bohdan Senyuk, Cuiling Meng, and Ivan I. Smalyukh*

Cite This: https://doi.org/10.1021/acs.langmuir.2c00611

Read Online

ACCESS | Metrics & More | Article Recommendations

ABSTRACT: Colloidal systems are abundant in technology, in biomedical settings, and in our daily life. The so-called "colloidal atoms" paradigm exploits interparticle interactions to self-assemble colloidal analogs of atomic and molecular crystals, liquid crystal glasses, and other types of condensed matter from nanometer- or micrometer-sized colloidal building blocks. Nematic colloids, which comprise colloidal particles dispersed within an anisotropic nematic fluid host medium, provide a particularly rich variety of physical behaviors at the mesoscale, not only matching but even exceeding the diversity of structural and phase behavior in conventional atomic and molecular systems. This feature article, using primarily examples of works from our own group, highlights recent developments in the design, fabrication, and self-assembly of nematic colloidal particles, including the capabilities of preprogramming their behavior by controlling the particle's surface boundary conditions for liquid crystal molecules at the colloidal surfaces as well as by defining the shape and topology of the colloidal particles. Recent progress in defining particle-induced defects, elastic multipoles, self-assembly, and dynamics is discussed along with open issues and challenges within this research field.

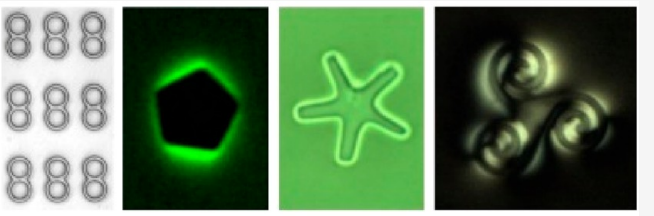

INTRODUCTION

Colloidal and liquid crystalline systems are classic examples of soft condensed matter, exhibiting structural similarities with the forms of self-organization found in both living organisms and in solid-state materials.[1,2] Nematic liquid crystals (LCs) are fluids having anisotropic properties stemming from the spontaneous, long-range orientational order of their constituent anisotropic molecules.[2] Their utility in electro-optic devices, such as LC displays, arises from their large birefringence and strong coupling to external fields and confining surfaces.[2,3] The use of nematic LCs as fluid hosts for colloidal dispersions enriches colloidal behavior due to anisotropic molecular interactions at colloidal surfaces and particle-induced defects and elastic distortions of the LC order.[4−27] Molecular interactions of rod-like LC molecules at the interface of another material result in energetically preferred alignment directions of the molecules at that interface.[28−46] Known as surface anchoring, this anisotropic interaction at LC surfaces defines surface boundary conditions and plays a key role in electro-optic applications involving LCs and in nematic colloidal self-assembly.[47−49] Surface anchoring[2,3] is one of the most important properties of LCs because of its relevance in practical applications. For instance, chemically and topographically patterned surfaces[50,51] have provided promising avenues for LC applications in displays, chemical sensing, biodetection, colloidal self-assembly,[52−64] and electro-optics.[3,47−49] Moreover, the properties of colloidal particles suspended in LCs are largely dependent upon the type and strength of the surface anchoring at their surfaces. For example, micrometer-scale spherical colloids that promote the anchoring of the LC molecules normal to the surface of the colloid can give rise to elastic deformations of the orientational order, which have either dipolar or quadrupolar symmetry depending upon the location and type of topological defects that accompany the particle.[8,17,18,25,52−58] The spatial dependence of the average alignment direction of the rod-like LC molecules is typically represented with a unit vector field, $\mathbf{n}(\mathbf{r})$, called the director field. Almost any surface in contact with the LC, including solid, liquid, and free surface, forces the director $\mathbf{n}(\mathbf{r})$ at the interface to orient in a specific direction, and then the alignment of LC molecules preset by boundary conditions propagates over large distances into the LC bulk.[2,3] There are three main types of the LC director $\mathbf{n}(\mathbf{r})$ alignment at the surfaces: homeotropic, planar, and tilted. Alignment is called homeotropic or planar when $\mathbf{n}(\mathbf{r})$ is forced to be, respectively, normal or tangential to the surface. The alignment is called tilted when the orientation of the director is somewhere between normal and tangential alignment. The preferred orientation of $\mathbf{n}(\mathbf{r})$ at the interface and the strength of surface anchoring is determined by the properties of the surfaces in contact with the LC. Besides the type and strength of surface anchoring, the detailed $\mathbf{n}(\mathbf{r})$ configuration surrounding a colloidal particle can depend on its shape, topology, confinement, the presence of external fields, as well as the bulk elastic properties of the LC host medium. Since the dominant anisotropic interactions that colloids experience

Received: March 11, 2022
Revised: July 10, 2022

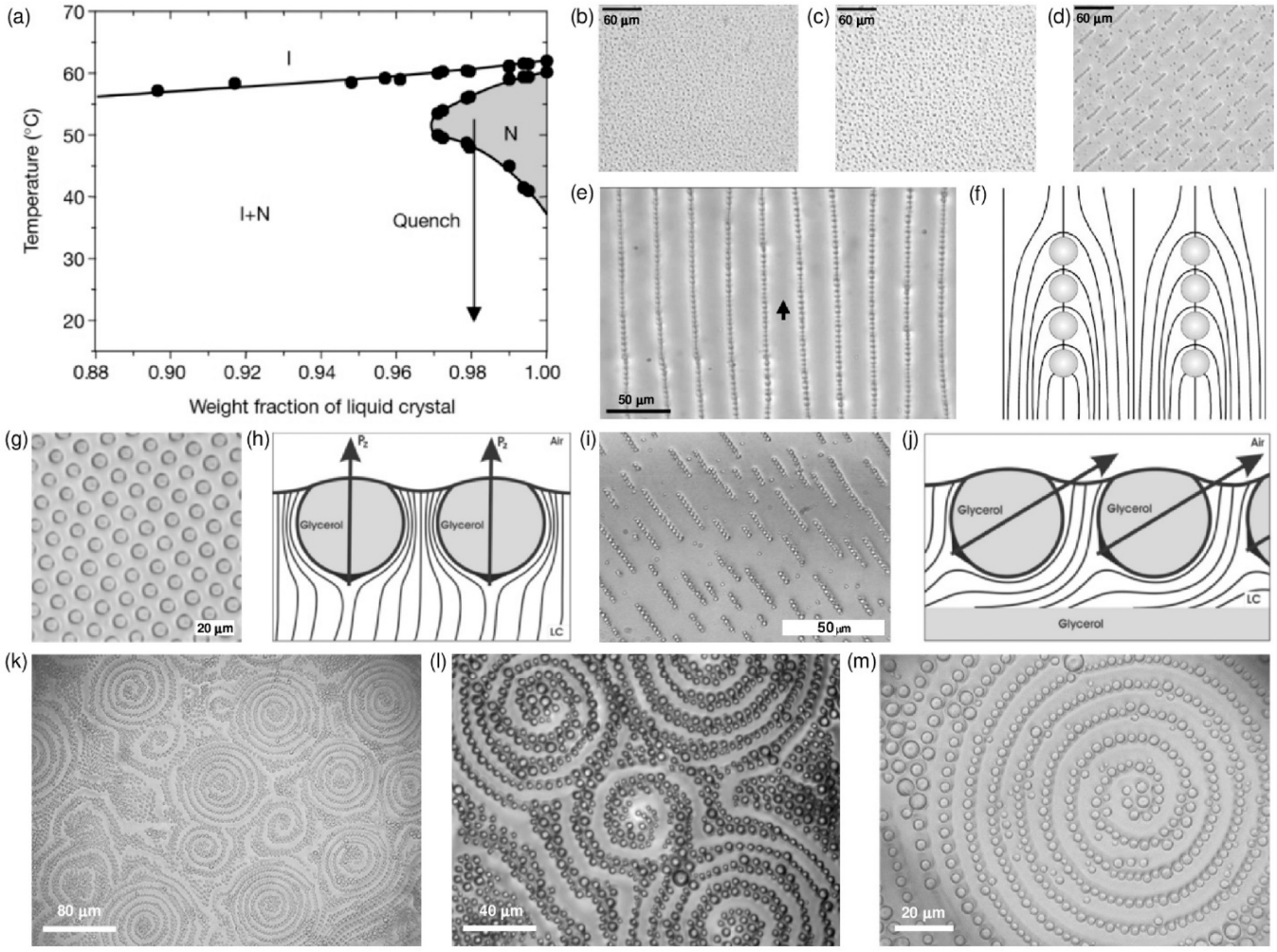

Figure 1. Nematic colloids obtained through phase separation. (a) Phase diagram of a mixture of a silicon oil in LC, which exhibits isotropic I and nematic N phases and biphasic (I + N) state. In the experiment, the mixture is cooled from the N region (gray area) to 20 °C, as shown by the arrow, to obtain isotropic silicone oil droplets in a nematic matrix by phase separation of dissolved silicone oil. (b) Droplets form after cooling (20 s after the quench). (c) Droplets diffuse randomly and coalesce in the initial stages of the separation (42 s after the quench). (d) Chains of droplets grow as time elapses (120 s after the quench). (e) Ordered chains of oil droplets. Black arrow indicates a rubbing direction. (f) Schematic diagram of $\mathbf{n}(\mathbf{r})$-distortions around particles in nematic LC. Black lines show the preferential orientation of LC molecules. Adapted with permission from ref 6. Copyright 2000 Springer Nature. (g–j) Optical microscopy pictures of glycerol droplets with a diameter of 7 μm forming (g) hexagonal structures at a free surface of a 60 μm thick LC layer and (i) chains at a free surface of a 7–10 μm thin nematic layer. (h, j) Corresponding schematic diagrams of $\mathbf{n}(\mathbf{r})$ in the top part of a LC layer. Adapted with permission from ref 65. Copyright 2019 American Physical Society. (k–m) Optical microscopy textures of glycerol droplets forming spirals on the surface of a cholesteric LC layer.

within the LCs arise from orientational elasticity, the types of ordered low elastic energy structures that are possible can be controlled through appropriate changes of colloids' surface topography and chemical properties. For conventional LCs, the established techniques that provide control over surface anchoring involve altering the physical and chemical properties of the interface either though the deposition and subsequent processing of polymer or inorganic films or through the formation of surfactant or phospholipid monolayers. For example, a standard method to define uniform, planar anchoring on a glass surface is to deposit a thin polymer layer, such as polyimide or poly(vinyl alcohol),[2] and mechanically buff the film using a fine pile velour. The surface boundary conditions can be also controlled on colloidal particle surfaces, along with controlling particle shapes,[59,61,62] topology,[60] surface charging,[63,64] and topography, etc.[25] This article provides an overview of different means of controlling LC–colloidal interactions to define the types of induced defects and distortions, elastic colloidal multipoles, colloidal self-assembly, and out-of-equilibrium behavior. Using examples from our own research, we discuss how various types of nematic LC colloids can be obtained by varying the chirality of the particles and host LC medium, by changing the particle shapes and surface topology, by controlling the strength of anchoring and easy axis orientations and patterns on colloidal surfaces, and so on.

LIQUID CRYSTAL COLLOIDS FABRICATION METHODS

Nematic Colloids Obtained through Phase Separation. The isotropic droplets of silicone oil in the bulk of a LC can be obtained as in refs 4–6, 9, and 12 using a mixture of "silicone oil" [poly(dimethylsiloxaneco-methylphenylsiloxane)] and such nematic LCs as, for example, a room temperature nematic E7. This mixture forms a homogeneous isotropic I phase at high temperatures and is in a biphasic state (I + N) at low temperatures (Figure 1a). A nematic N phase is stable at intermediate temperatures when the concentration of silicone

https://doi.org/10.1021/acs.langmuir.2c00611
Langmuir XXXX, XXX, XXX–XXX

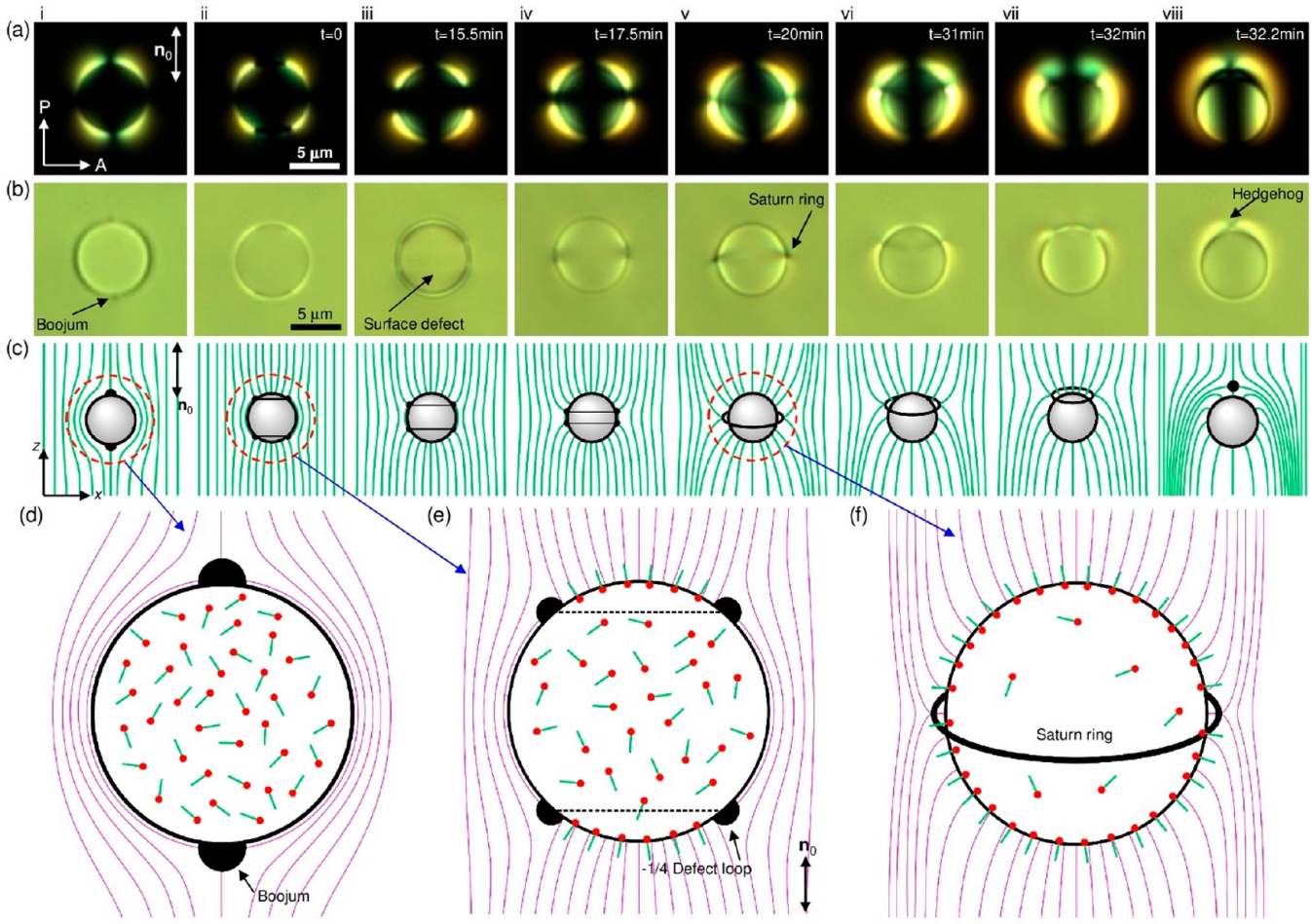

Figure 2. Transition from tangential to homeotropic boundary conditions, and corresponding transformations of elastic multipoles around glycerol droplets. (a) Polarizing and (b) bright-field microscopy images of elastic multipoles, and (c) corresponding schematics of $\mathbf{n}(\mathbf{r})$ during transformations; P and A show crossed polarizer and analyzer, and $\mathbf{n}_0$ is a far-field director. (d) Schematics showing the mechanism of the anchoring transition at the LC−glycerol droplet interface. Adapted with permission from ref 46. Copyright 2021 American Association for the Advancement of Science.

oil is low. In the isotropic I and nematic N phases, the silicone oil is homogeneously dissolved in E7. This mixture of E7 and silicone oil can be filled in between two glass slides separated by thick (several tens of micrometers) spacers. Before the mixture is added into the experimental cells, the glass can be coated with poly(vinyl alcohol), polyimide, or other alignment layers and rubbed to cause the N continuous phase to become homogeneously aligned along a far-field director $\mathbf{n}_0$. After filling into a cell placed onto a temperature-controlled stage of, for example, an optical microscope, the system is cooled from the N phase (gray area in Figure 1a) into the biphasic state (I + N) at about 20 °C (Figure 1a). When a sample is cooled from the N to the (I + N) state, phase separation occurs as the uniform single-phase mixture is not thermodynamically stable at lower temperatures. As a result, small isotropic droplets of silicone oil form in the nematic and grow through coalescence when they diffuse and collide (Figure 1b). When the size of the droplets reaches some critical size $R^* = K/W$ of several micrometers, where K is the average elastic constant of the LC and W is the surface anchoring strength, the coalescence stops and droplets start attracting each other, like electrostatic dipoles,[4,8,25] forming linear chains oriented along $\mathbf{n}_0$ (Figure 1c and 1d). Experimental observations reveal that the boundary conditions on the surface of the droplets are normal for LC molecules, a dipolar configuration of $\mathbf{n}(\mathbf{r})$ deformations is formed around the droplets (Figure 1f), and they form long chains along the far-field director $\mathbf{n}_0$ (Figure 1e and 1f).

The isotropic droplets on the surface of a LC can be also obtained using glycerol (clear viscous fluid) as in refs 10 and 65. A glass Petri dish containing a millimeters-thick layer of glycerol and a thin layer of a nematic LC pentylcyanobiphenyl (5CB) on top is kept at 50 °C for tens of minutes, facilitating diffusion of glycerol molecules into the micrometers-thick 5CB layer which is in the isotropic phase slightly above 35 °C. After the sample is cooled down, the solubility of glycerol decreases and glycerol droplets start appearing and growing. The technique allows producing droplets of a constant radius, which is determined by the cooling rate. The formed droplets are trapped on the surface of a LC at the air−LC interface as can be unambiguously determined using, for example, fluorescence confocal polarizing microscopy (FCPM).[11] A several hours relaxation at room temperature results in 2D ordered structures of initially randomly distributed droplets (Figure 1g−j). The surface of the glycerol droplets promotes tangential alignment of LC molecules (Figure 1h and 1j). When the LC layer is thick so that the layer thickness is much larger than the droplets dimensions, the order of the formed ordered structure is hexagonal (Figure 1g and 1h). In thin LC films, when the layer thickness is comparable to several radii of droplets, the pattern changes to droplets forming chains aligned along the average in-plane $\mathbf{n}(\mathbf{r})$ projection. The length of the chains increases when the LC layer thickness decreases. Both hexagonal and chain organizations disappear when 5CB is heated again into the isotropic phase.

Colloidal particles follow the director orientation in nematic LCs as can be seen from Figure 1d and 1e. Subsequently, they also follow the local director orientations in a twisted structure of LC if the amount of twist is much larger than the particle's dimensions. In a similar way as in the case of glycerol droplets on the surface,[10,65] the phase separation method can be used to obtain small glycerol droplets in cholesteric LCs (Figure 1k−m). Cholesteric LCs can be obtained by mixing a small amount of cholesteric dopants, cholesteryl pelargonate or CB15, for

https://doi.org/10.1021/acs.langmuir.2c00611
Langmuir XXXX, XXX, XXX−XXX

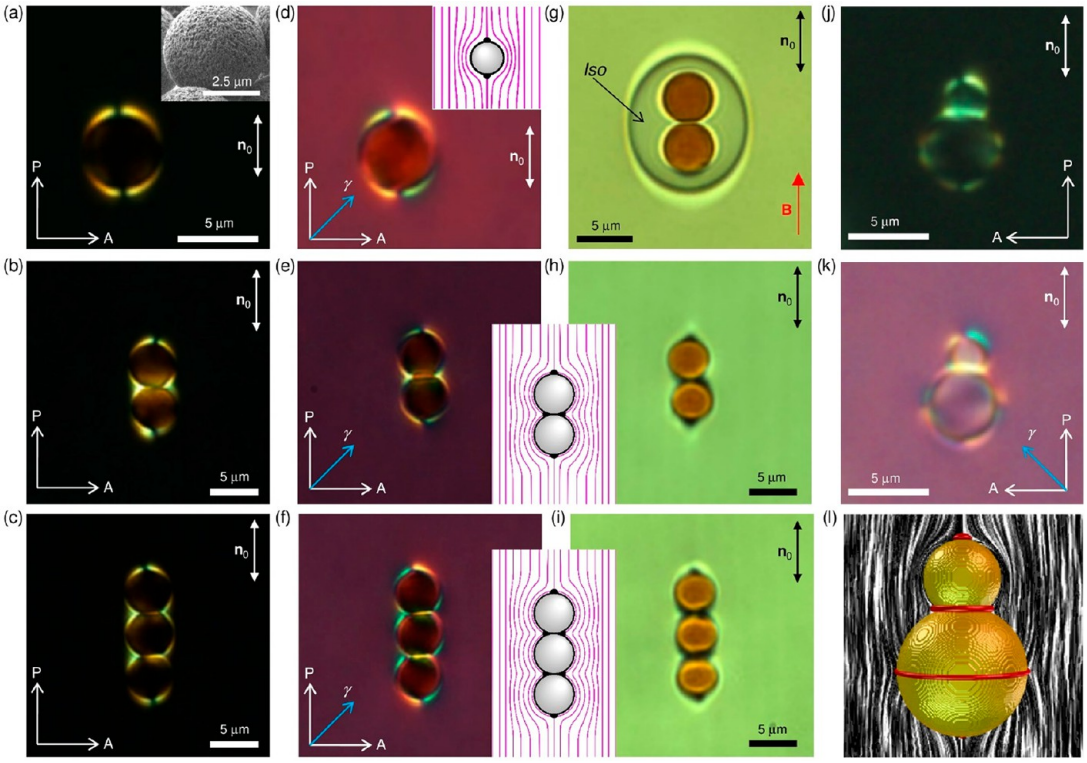

Figure 3. Spherical and anisotropic solid particles. (a–i) Textures of colloidal particles in a nematic obtained with (a–f) optical polarizing, (d–f) with and (a–c) without a retardation plate, and (g–i) bright-field microscopy; γ marks a slow axis of a full wave (530 nm) retardation plate, and B shows the magnetic field. (Inset in a) SEM image of epoxy particles. (Insets in d–f) Schematic diagrams of $\mathbf{n}(\mathbf{r})$ (magenta lines). (j–l) Anisotropic gourd-shaped particle: (j, k) Textures of a gourd-like particle in a nematic cell from optical polarizing: (j) without and (k) with a retardation plate. (l) Corresponding calculated $\mathbf{n}(\mathbf{r})$ around a gourd-shaped particle. Adapted with permission from ref 70. Copyright 2019 Springer Nature.

example, into a nematic 5CB to achieve a long-pitch cholesteric phase. Because of the hybrid boundary conditions where LC molecules are tangential to the glycerol–LC interface while orienting normally at the air–LC interface, cholesteric textures form a system of concentric spirals and isotropic droplets form long chains spiraling accordingly with the orientation of the local director (Figure 1k–m).[12]

Intrinsically, as described above, pure silicon oil and glycerol droplets impose, respectively, homeotropic and tangential LC alignment at their interface inducing in a LC so-called elastic dipoles (Figures 1f and 2cviii) and quadrupoles (Figure 2ci and 2cv).[8,25] However, one can also modify and control the boundary conditions at the surface of fluid droplets by mixing specific additives like in ref 46. Spherical micrometer-size droplets of isotropic fluid in the bulk of a nematic LC can be obtained by mixing a small amount (~1–5 vol %) of glycerol with a nematic LC and vigorous agitation such as flicking or sonication. A spherical shape of droplets when mixed with the LC is reinforced by the high interfacial tension between two media. Droplets of pure glycerol dispersed in a nematic LC ZLI-2806 promote planar azimuthally degenerate boundary conditions at the interface between the LC and glycerol. This induces a quadrupolar configuration of $\mathbf{n}(\mathbf{r})$ around the droplet (Figure 2ai, 2bi, 2ci, and 2d) with two surface point defects called "boojums" at the poles of the droplet along $\mathbf{n}_0$. Boojum quadrupoles obtained with pure glycerol and the corresponding $\mathbf{n}(\mathbf{r})$ configuration are stable over long periods of time. However, adding a trace amount of surfactant to glycerol before mixing it with the LC modifies the boundary conditions and changes the behavior of this droplet-induced elastic multipole. For example, surfactant sodium dodecyl sulfate (SDS) at small concentrations uniformly dissolves within glycerol. Larger concentrations of SDS (>0.1 wt %) promote homeotropic boundary conditions at the surface of the droplets, resulting in a dipolar $\mathbf{n}(\mathbf{r})$ configuration with a bulk point defect called "hedgehog" (Figure 2aviii, 2cviii, and 2bviii).[8] At small concentrations of SDS (<0.1 wt %), the droplets initially, right after the preparation, appear as boojum quadrupoles with tangential boundary conditions (Figure 2ai, 2ci, 2bi, and 2d), but configurations of $\mathbf{n}(\mathbf{r})$ and singular defects change over long time. In the beginning, two boojums at the poles start opening into the surface defect loops encircling the surface of the droplet close to its poles (Figure 2c and 2e). As time goes on, these surface defect loops slowly drift away from the poles and, upon reaching the equator, combine to form a single bulk defect loop called a "Saturn ring"[8,25] and the corresponding quadrupolar $\mathbf{n}(\mathbf{r})$ configuration (Figure 2av, 2cv, 2bv, and 2f). After some time, the Saturn ring moves toward one of the poles of the droplet, eventually transforming into a bulk point defect hedgehog (Figure 2aviii, 2cviii, and 2bviii).[8,25] The polarizing and bright-field microscopy textures and corresponding schematics of $\mathbf{n}(\mathbf{r})$ (Figure 2a, 2b, and 2c, respectively) display details of these transformations. Tangential-to-homeotropic changes of the patchy boundary conditions at the interface between the LC and glycerol cause these (Figure 2) experimentally observed topological transformations of elastic multipoles studied in detail in ref 46.

Spherical and Anisotropic Solid Particle Synthesis. Most of the studies of LC colloids deal with solid spherical particles.[8,25,29−45,52−58,65−67] Typically, to obtain solid spherical colloids with homeotropic anchoring at the surface, silica or glass colloids are used additionally treated with an aqueous or alcohol solution (0.05 wt %) of *N*,*N*-dimethyl-*N*-octadecyl-3-aminopropyl-trimethoxysilyl chloride (DMOAP).[25,33−35,55] Different polymer-based solid spherical particles, like melamine resin particles, intrinsically provide tangential boundary conditions for LCs.[67] Silica particles treated with 3-methylaminopropyl trimethoxysilane (MAP) also provide tangential boundary conditions.[42,55,68]

To demonstrate how the shape and boundary conditions on the surfaces of colloidal particles dictate the structure of the surrounding $\mathbf{n}(\mathbf{r})$-deformations and to identify the "design recipes" for obtaining the desired elastic multipoles and the ensuing elasticity-mediated interactions, there is a demand for colloids which are anisotropic in terms of shape and anchoring at their surface.

https://doi.org/10.1021/acs.langmuir.2c00611
Langmuir XXXX, XXX, XXX−XXX

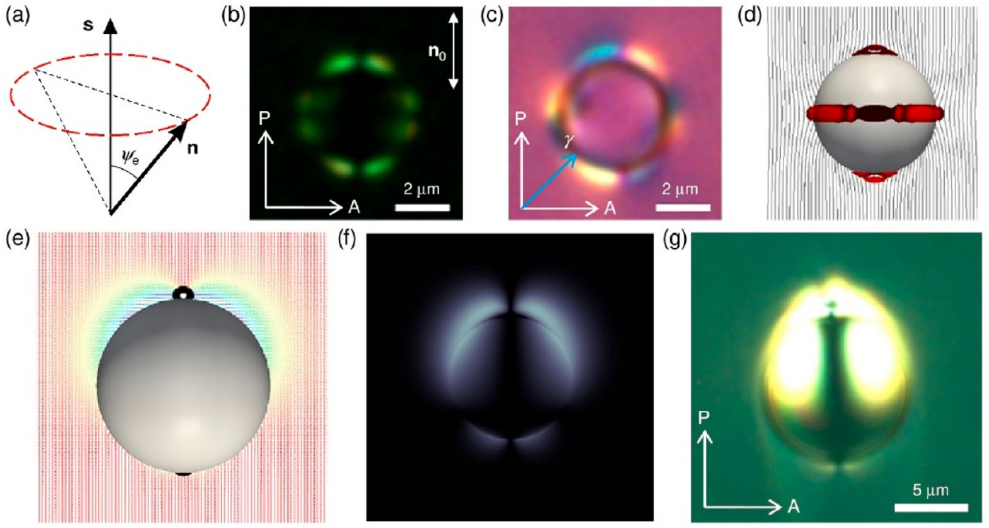

Figure 4. Conic degenerate anchoring at the particles' surface. (a) Schematic of the conic degenerate surface boundary conditions with the "easy axis" **n** at a constant angle ψ_e to a local normal **s** to the surface. (b, c) Optical micrographs of elastic hexadecapoles obtained with polarizing microscopy. Adapted with permission from ref 66. Copyright 2016 Springer Nature. (d) Schematic diagram of induced $\mathbf{n}(\mathbf{r})$ satisfying the tilted boundary conditions at the polystyrene microspheres surface. (e) Calculated director fields for elastic conic anchoring dipole colloids. Defects are shown in black. (f) Corresponding simulated polarized light micrographs of dipole colloids with a tilt angle $\psi_e = 45°$. (g) Optical microscopy texture of a dipole with conic anchoring, which is consistent with calculated textures shown in e and f. Adapted with permission from ref 76. Copyright 2019 Springer Nature.

Table 1. Examples of Boundary Conditions Induced by Colloidal Particles

liquid crystal	material of colloidal particle	alignment agent	boundary conditions
5CB	silica	DMOAP	homeotropic[55,60]
5CB	silica	MAP	planar[55]
5CB	borosilicate glass	DMOAP	homeotropic[34,70]
5CB, ZLI-2806	melamine resin	no treatment	planar[67]
5CB, E7	polystyrene	no treatment	planar[67,70]
MJ032358	polystyrene	DMOAP	homeotropic[15]
E7	silicone oil	pristine	homeotropic[6]
5CB, ZLI-2806	glycerol	pristine	planar[46]
ZLI-2806	glycerol	mixed with SDS	homeotropic[46]
5CB	glycerol	mixed with SDS	tilted[76]
5CB	β-$NaYF_4$:Yb/Er	no treatment	homeotropic[79]
5CB	β-$NaY_{0.5}Gd_{0.3}Yb_{0.18}Er_{0.02}F_4$	Si-PEG	planar[78]
5CB	epoxy based	no treatment	planar[69]
5CB	photoresist SU-8	no treatment	planar[59]
5CB	photoresist SU-8	DMOAP	homeotropic[40]

An experimentally accessible example of anisotropic colloids can be composite colloidal particles consisting of spherical elements of similar size and boundary conditions (Figure 3b, 3c, and 3e–i). Epoxy-based spherical superparamagnetic beads[69] can be used to fabricate dimers, trimers, tetramers, and so on (Figure 3b, 3c, and 3e–i) in order to induce $\mathbf{n}(\mathbf{r})$-structures, which correspond to various higher order elastic multipoles.[70] Superparamagnetic beads define the planar boundary conditions for LC molecules as can be observed from polarizing optical microscopy textures (Figure 3a and 3d). Magnetic nanoparticles embedded into superparamagnetic beads allow for easy control of the beads' orientation with a magnetic field.[69,71] To fabricate composite linear particles consisting of two or more superparamagnetic beads, individual beads are placed nearby each other using optical tweezers and, with the same optical tweezers, the LC is locally melted to the isotropic state close to the beads. Beads trapped in the melted isotropic region of a LC sample can be easily arranged into linear chains of two or more touching beads using optical tweezers, and then these chains can be easily aligned parallel to a preset $\mathbf{n}_0$ using holonomic magnetic control[69] (Figure 3g). In this way, they irreversibly form dimers, trimers, or tetramers. When the locally isotropic LC is cooled to the nematic phase, the magnetic field holding chains of beads along $\mathbf{n}_0$ can be removed, leaving formed dimers, trimers, or tetramers stable and oriented along $\mathbf{n}_0$ (Figure 3b, 3c, and 3h–i). The alternating director tilt at particle surfaces with respect to $\mathbf{n}_0$ uncovered by different modes of microscopy is consistent with that in the ansatzes of sources of high-order elastic multipoles. Even though a single superparamagnetic bead induces an elastic quadrupole (Figure 3a and 3b), a pair of superparamagnetic beads in a chain oriented parallel to $\mathbf{n}_0$ (Figure 3b, 3e, and 3h) has a strong elastic hexadecapole moment, which can be the strongest leading order elastic multipole for certain parameters of a dimer. Similarly, a chain of three particles can possess a strongly pronounced 64-pole (Figure 3c, 3f, and 3i).[71]

Dimers of spherical particles (Figure 3j) are also good sources of elastic distortions as they allow for more complex distortions of $\mathbf{n}(\mathbf{r})$ than what can be induced just by individual colloidal spheres and also because they can be mass produced using wet chemistry approaches.[72−74] Thus, elastic multipoles formed around colloidal particles consisting of two dissimilar spheres having different sizes, composition, and anchoring are of special interest. Gourd-shaped colloidal particles[70,75] consist of two lobes of different diameter and with different surface anchoring boundary conditions for $\mathbf{n}(\mathbf{r})$ (Figure 3j–l). The dissimilar boundary conditions are defined through the

https://doi.org/10.1021/acs.langmuir.2c00611
Langmuir XXXX, XXX, XXX−XXX

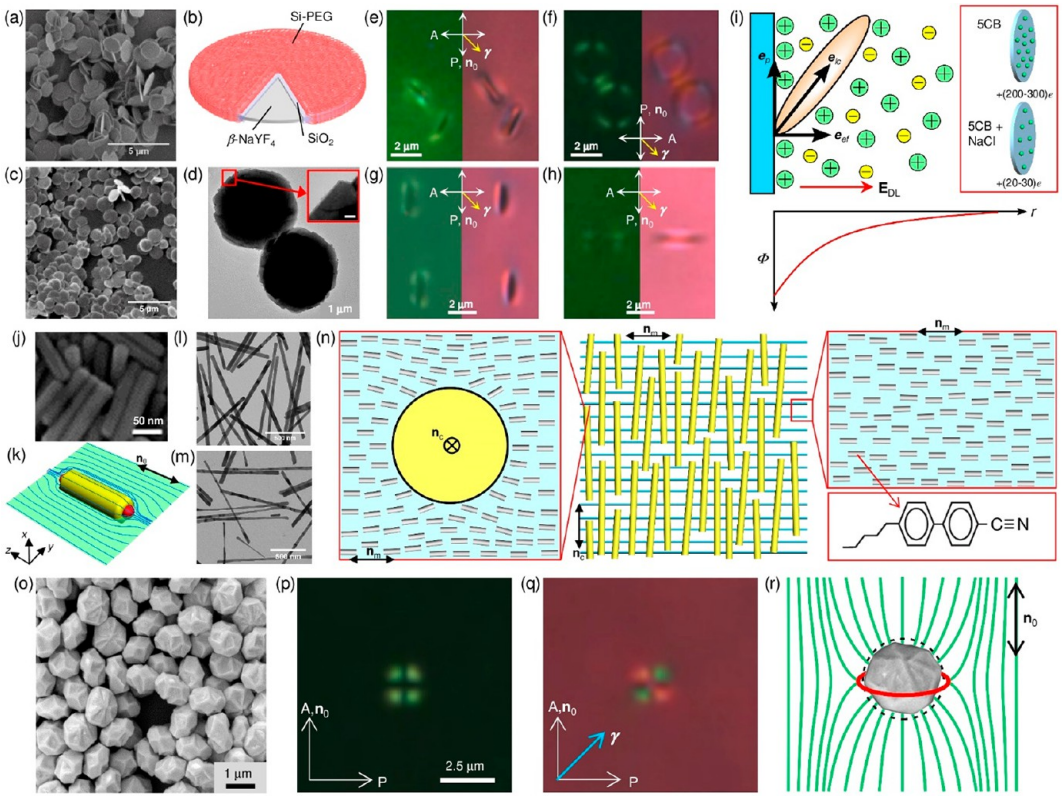

Figure 5. Solid charged nanoparticles: SEMs of platelets before (a) and after (c) SiO_2 coating. (d) TEM micrograph of platelets. (Inset) SiO_2 layer which is visible at the platelet's edge as a thin gray stripe. (b) Schematic of platelets showing a core, SiO_2 coating, and Si-PEG alignment layer. (e–h) Optical microscopy textures of platelets with (e) conic, (f, g) planar, and (h) perpendicular surface anchoring under crossed polarizers (left) without and (right) with a retardation plate γ in a nematic cell. (i) Effect of the ionic content of LC medium showing a schematic diagram of LC alignment (an ellipsoid) at the surface (blue); $\mathbf{e}_p$, $\mathbf{e}_{ef}$ and $\mathbf{e}_{lc}$ show easy axes determined by interactions with the polymer capping, electrostatic interactions, and the LC alignment resulting from their competition, respectively. Φ is an electric potential varying over the thickness of the double layer, and r is the distance from the platelet surface. Red arrow shows the direction of electric field $\mathbf{E}_{DL}$. Positive and negative charges are shown, respectively, by green and yellow filled circles. Right-side insets schematically show the density of a positive charge (green spheres) at the platelet surface in a doped 5CB. Adapted with permission from ref 63. Copyright 2019 American Association for the Advancement of Science. (j) SEM image of small nanorods. (k) Schematic illustration of $\mathbf{n}(\mathbf{r})$ (blue) around a single nanorod (yellow), with red hemispheres at poles depicting two boojums. Adapted with permission from ref 78. Copyright 2016 American Association for the Advancement of Science. (l, m) TEMs of nanorods (l) before and (m) after acid treatment. (n) Schematic representation of the hybrid molecular-colloidal nematic LC, with the insets showing (top right) molecular ordering and (bottom right) chemical structure of a 5CB molecule and left inset showing a schematic representation of $\mathbf{n}(\mathbf{r})$ around a nanorod with soft perpendicular boundary conditions. Adapted with permission from ref 79. Copyright 2018 American Association for the Advancement of Science. (o) SEM image of dumpling colloidal particles. (p, q) Polarizing microscopy textures of dumpling particles with homeotropic anchoring in a planar nematic cell between crossed polarizers (q) with and (p) without a retardation plate. (r) Schematic diagram of $\mathbf{n}(\mathbf{r})$ (green lines): red circle indicates a singular defect loop Saturn ring. Adapted with permission from ref 80. Copyright 2021 American Association for the Advancement of Science.

synthesis of dimers, in which cross-linked polystyrene spherical seeds (a smaller lobe) were swollen with styrene and the elastic contraction of the cross-linked polystyrene expels styrene out of the swollen seeds to give rise to the second (larger) lobe.[73−75] The smaller particle's lobe has tangential anchoring, while the larger lobe has conic anchoring,[66,76] as can be seen from the polarizing microscopy textures of such particles in a LC (Figure 3j and 3k) with a calculated director structure around the particle (Figure 3l).[70] When mixed with a LC, gourd-shaped dimers align with their cylindrical symmetry axis parallel to $\mathbf{n}_0$ and induce two boojums, one at the south pole of a large lobe and another at the north pole of a smaller lobe, as well as a surface defect loop at the larger lobe's equator (Figure 3j–l). A singular defect loop resulting from the mismatch in the alignment of molecules at both lobes in the point of contact is also visible traversing around the contact line between the two lobes. Director structures around such particle depend on multiple geometrical parameters like the radii of both lobes, the distance between their centers, etc.[70]

Colloidal particles with conic degenerate surface anchoring,[66,76,77] where the boundary conditions promote the alignment of LC molecules at some angle between tangential and normal alignment (Figure 4a), are worthy of special mention. Colloidal particles with conic boundary conditions give a rise to new elastic multipoles called elastic hexadecapoles[66,76] (Figure 4b–d) and elastic dipoles with conic anchoring (Figure 4e–g).[76] Conic anchoring at the surface of glycerol droplets in a nematic LC 5CB (Frinton Laboratories, Inc.) (Figure 4f) can be achieved with a small amount (<0.1 vol %) of a molecular surfactant SDS mixed with glycerol.[76]

Surface Charging and Electrostatic Anchoring. Boundary conditions at the colloids' surface determine $\mathbf{n}(\mathbf{r})$-deformations around the colloidal particles immersed into LC and formation of the corresponding elastic multipoles.[8,25,70] Therefore, controlling the boundary conditions especially when colloids already are mixed in the dispersions can affect the self-assembly of colloidal particles resulting in different fluid materials with new symmetry.[78−82] Examples of boundary conditions that can be obtained for LC molecules using specific alignment agents at different colloidal particles described in this article are summarized in Table 1. One of the methods of controlling the type of anchoring at the colloids' surface is using electrostatic charging of their surface (Figure 5).

https://doi.org/10.1021/acs.langmuir.2c00611
Langmuir XXXX, XXX, XXX−XXX

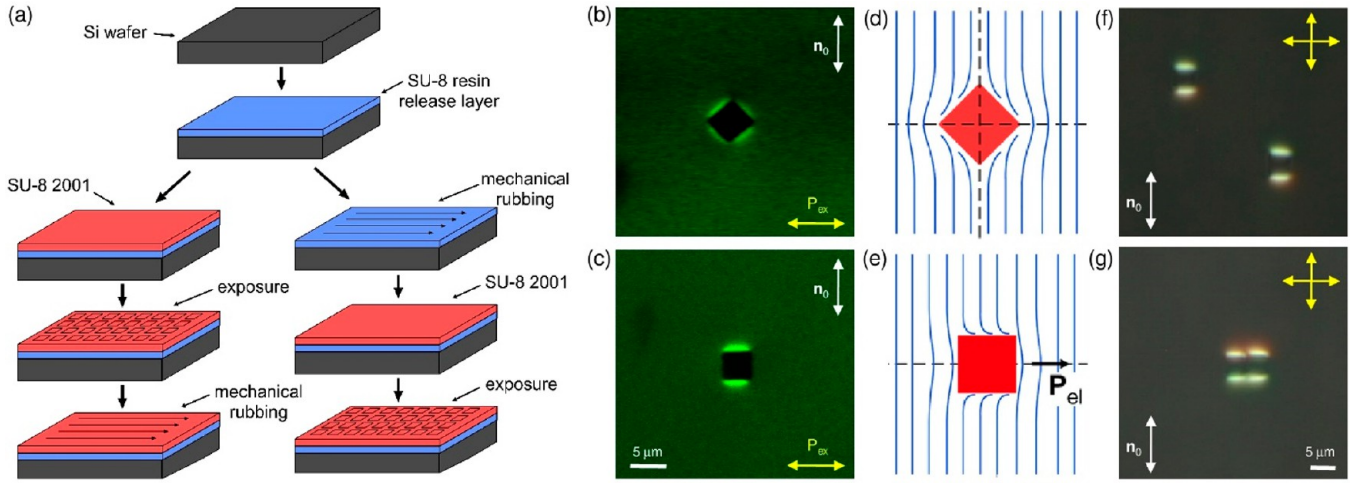

Figure 6. Defining shape and boundary conditions of lithographically produced colloids. (a) Schematic illustration showing a process to define the nematic anchoring direction on lithographic colloidal particles via mechanical rubbing on (left) their top surfaces and (right) their bottom surfaces. (b) Three-photon excitation fluorescence polarizing microscopy (3PEF-PM) image reveals that untreated square-shaped platelets with degenerate planar anchoring align with one diagonal parallel to $\mathbf{n}_0$, accompanied by four bright lobes corresponding to the distorted director field. (c) Similar image for a particle with surfaces rubbed parallel to two out of four edge faces of the particle. (d) Schematic of the quadrupolar $\mathbf{n}(\mathbf{r})$ (blue lines) surrounding the square-shaped platelet with tangentially degenerate anchoring. Dashed lines show two mirror symmetry planes orthogonal to the platelet's large-area faces (third mirror symmetry plane passes through the platelet's midplane). (e) Corresponding schematic for a platelet with rubbed surfaces, which align with that rubbing direction parallel to $\mathbf{n}_0$, giving rise to the dipolar $\mathbf{n}(\mathbf{r})$ with elastic dipole moment $\mathbf{P}_{el} \perp \mathbf{n}_0$. (f, g) Polarizing optical micrographs of elastic colloidal dipoles formed by two rubbed square platelets when (f) far apart and (g) self-assembled into a colloidal dimer.

Solid semiconductor colloidal particles with surface charging are prepared using the hydrothermal synthesis method.[83−85] Varying the concentrations of oleic acid and NaOH, nanorods of different lengths (Figure 5j and 5l)[78,79] and dumpling nanoparticles[80] (Figure 5o) can be synthesized. For synthesis of platelets,[63,81] oxalic acid is used instead of oleic acid.

Semiconductor solid β-$NaYF_4$:Yb,Er platelets (Figure 5a−h) can be synthesized following the procedures described in refs 63 and 81. The synthesis yields circular plates with a thickness of about 20 nm and an average diameter of 2 μm (Figure 5a and 5c). For surface treatment, 1 mL of an aqueous dispersion of particles is mixed with 5 mL of hydrogen peroxide and 100 μL of nitric acid and kept stirring overnight, which ensures complete removal of the oxalic acid from the particle surface, leaving the particles positively charged. Then, the uncapped platelets are precipitated from the solution by centrifugation and dispersed in 1 mL of ethanol. Next, the platelets are covered with a thin layer of silica (SiO_2). To achieve this, 300 mg of polyvinylpyrrolidone (PVP; M_w 40 kDa) is dissolved in 4 mL of ethanol by ultrasonication, and 1 mL of the platelets dispersion in ethanol is added to this solution and kept stirring for 24 h. Thus, PVP ligands, which favor silica growth, adsorb to the particle surface. Particles coated with PVP are separated from the solution using centrifugation and redispersed in 5 mL of ethanol. After that, 250 μL of ammonia solution (28 wt % in water) is added to the dispersion, which is followed by 8 μL of tetraethyl-orthosilicate (TEOS) with continuous agitation for about 12 h. Obtained dispersions of silica-coated particles are centrifuged at 6000 rpm for 5 min and redispersed in 5 mL of ethanol. Next, 2 mL of an ammonia solution is added to the mixture, bringing the pH of the solution to about 12, which is immediately followed by adding 1 mL of hot methoxy polyethylene glycol silane (Si-PEG; M_w 5 kDa) solution in ethanol (25 mg/mL) under constant agitation and kept for 12 h. Later, the resulting Si-PEG-functionalized particles are precipitated by centrifugation, washed with deionized water several times, and redispersed in 1 mL of ethanol for subsequent use. Thus, the synthesis conditions described above result in a SiO_2 layer thickness of 5 nm (Figure 5d), but the SiO_2 thickness can be tuned by varying the concentration of TEOS in the reaction (Figure 5a, 5c, and 5d).[63,81] The measured surface charge on the obtained uncapped platelets was ∼+300e. However, the process of silica capping reduces the effective surface charge of the particles to +(100−200)e, showing that the charging on particles is dominated by positively charged cores of particles, although it can also be controlled by silica coating.[63]

The electrostatic contribution to the surface anchoring strength and coupling between normal to the surface $\mathbf{s}$ and $\mathbf{n}_0$ depend on the surface charge and ionic content of the LC, showing a tendency to orient molecules along and away from an easy axis $\mathbf{e}_p$ describing the natural coupling of $\mathbf{n}(\mathbf{r})$ with a Si-PEG-coated surface (Figure 5i). Depending on the grafting density, Si-PEG functionalization can promote homeotropic, planar, or conic boundary conditions (Figure 5e−h). For example, in the case of solid platelets (Figure 5a−d) immersed into a LC,[63,81] experimental optimization of grafting gives $\mathbf{e}_p$ parallel to the platelet to obtain the entire range of tilt θ = 0−90° because of the aligning effect of the electric double layer. When surface charging is small, molecules orient parallel to the particle surface (Figure 5f and 5g) due to a minimal electrostatic contribution to the surface energy strength. At high surface charging, LC molecules orient normal to the platelets' surface (Figure 5h), whereas conical boundary conditions emerge at moderate charging (Figure 5e).

Short semiconductor nanorods with the composition β-$NaY_{0.5}Gd_{0.3}Yb_{0.18}Er_{0.02}F_4$ (Figure 5j) can be synthesized as described in ref 78. After the synthesis, nanorods are collected and washed with ethanol and water and finally redispersed in cyclohexane. The nanorods attain positive charges after removal of the oleic acid molecules from their surfaces during the nanorod dispersion preparation, which is due to the protonation of particle surfaces in an acidic medium.[85] The surface charging of nanorods is tuned by controlled variation of the capping density of Si-PEG at the surface of the particles. The Si-PEG ligands help to define tangentially degenerate surface boundary conditions for the nematic LC director (Figure 5k) and also tend to reduce the surface charging of nanorods. The electrostatic charging can be controlled by varying the density of Si-PEG chains attached at the surface of semiconductor nanorods. Variation of the Si-PEG concentration and reaction time can be used to control the grafting density and thereby to tune the effective positive surface charging of the particles within ∼+(60−250)e per nanorod.[78] The dispersion of these nanorods with a LC at higher concentrations resulted in new triclinic nematic colloidal crystal materials.[78]

Long colloidal nanorods (Figure 5l and 5m) can be synthesized by the methods described in detail in ref 79. The obtained nanorods are positively charged. To ensure optimal stabilization of the nanorods in

https://doi.org/10.1021/acs.langmuir.2c00611
Langmuir XXXX, XXX, XXX−XXX

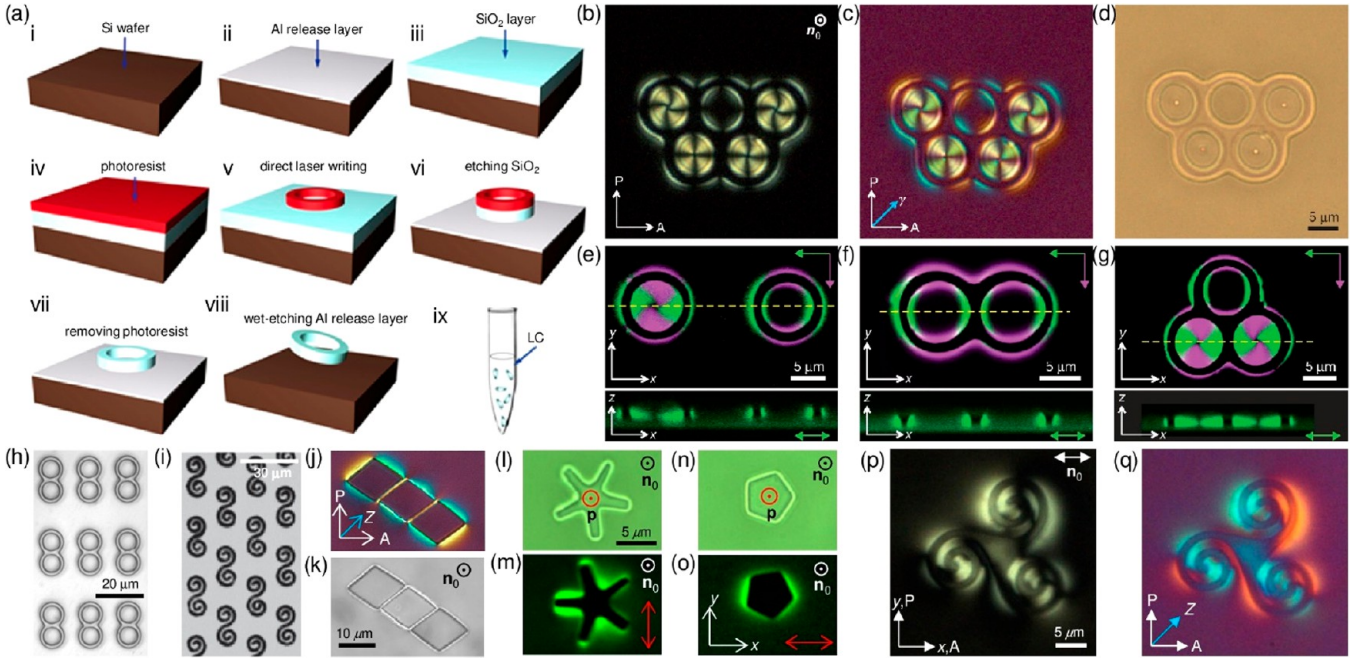

Figure 7. Colloidal particles fabricated by a direct laser writing method. (a) Schematic diagram of colloidal particles fabrication. (b–g) Colloidal handlebodies with homeotropic anchoring aligned orthogonal to $\mathbf{n}_0$: (b–d) $g = 5$ handlebodies and induced $\mathbf{n}(\mathbf{r})$-structures imaged by polarizing microscopy (b) without and (c) with a retardation plate, and (d) bright-field microscopy and (e–g) 3PEF-PM images. (e–g) 3PEF-PM textures of (e) single, (f) double, and (g) triple colloidal particles. Adapted with permission from ref 60. Copyright 2013 Springer Nature. Micrographs of arrays of (h) double handlebodies and (i) spiral silica colloidal particles on an aluminum layer obtained in the reflective mode of optical microscopy. (j–o) Polygonal truncated pyramids in a nematic LC. Optical micrographs of (j, k) rhombic, (l, m) star, and (n, o) pentagonal particles. Adapted with permission from ref 61. Copyright 2015 American Physical Society. (p, q) Polarizing micrographs of spiral particles with tangential anchoring in a planar nematic cell. Adapted with permission from ref 62. Copyright 2015 Royal Society of Chemistry.

the nematic LC, they are additionally treated with a hydrochloric acid (HCl, 38.0 wt %) solution. The typical average aspect ratio of the as-synthesized nanorods within a single synthesis batch is estimated to be ~45, with the example shown in Figure 5l. After the acid treatment, the surfaces of the nanorods are etched and the aspect ratio changes to within 60–110 (Figure 5m). Using such approaches in combination with adjustments of the synthesis process, the aspect ratio of the nanorods can be controlled within the range 40–110.[79] The bare nanorods can be dispersed in 5CB without the need of any further surface functionalization, and they spontaneously induce perpendicular boundary conditions for the 5CB molecular alignment and orient perpendicularly to the molecular director $\mathbf{n}_m$ of 5CB (Figure 5n) at different volume fractions of particles. The perpendicular orientation of the nanorods with respect to $\mathbf{n}_m$ is caused by homeotropic boundary conditions with weak surface anchoring at the surface of the nanoparticles.[86,87] Dispersion of long nanorods with homeotropic anchoring at certain concentrations results in hybrid molecular–colloidal LCs with biaxial D_{2h} orthorhombic symmetry.[79]

The typical synthesis for dumpling-like colloids (Figure 5o–r)[80] yields octanoic acid-functionalized dumpling-shaped particles with an average size of 1 μm, as can be seen from the scanning electron microscopy (SEM) micrograph of particles deposited onto a silicon substrate (Figure 5o). To induce positive surface charges, particles should be treated with an acidic solution.[80] To prepare the colloidal dispersions in a LC, the particles in an ethanol solution are mixed with a nematic 5CB followed by solvent evaporation at 70 °C for 2 h and cooling to a nematic phase under vigorous mechanical agitation. Judging from the polarizing microscopy images, the colloidal dumplings have homeotropic anchoring on their surfaces, and the symmetry of the resulting $\mathbf{n}(\mathbf{r})$-distortions around the particles (Figure 5p–r) is of the "quadrupolar" type[8,25] with an encircling disclination loop.

Photolithography as a Means of Controlling Colloidal Shapes. Colloidal particles with shapes different from spherical can offer distinct ways of controlling elasticity-mediated interactions and self-assembly in LCs and can be fabricated using photolithography methods.[59] To prepare colloidal particles by means of photolithography,[59,88,89] silicon wafers should be thoroughly cleaned.[59,60] Cleaned wafers are first coated with a release layer consisting of a 28 wt % solution of SU-8 epoxy resin dissolved in cyclopentanone, which results in 1 μm thick films after spin coating and removal of the solvent via soft baking (Figure 6a). A second 1 μm thick layer of photosensitive SU-8 2001 (Microchem) is spun on top of the release layer and soft baked. In order to define the planar anchoring direction on the bottom surfaces of lithographic colloids, release layers are unidirectionally rubbed against soft velour mounted on a flat surface as shown in Figure 6a, with the rubbing direction perpendicular to the single flat edge of the wafer, which is later utilized by the lithography system to orient the wafer relative to the features on the reticle mask. As shown schematically in Figure 6a, to fabricate lithographic colloids with their top surfaces rubbed, the release layer is not mechanically rubbed after soft baking, and the second photosensitive SU-8 layer is applied and mechanically rubbed after exposure. Photolithographic fabrication on a single wafer can yield up to ~10^8 particles with high monodispersity. After exposure, the wafers are immersed in SU-8 developer (1-methoxy-2-propyl acetate) and lightly ultrasonicated dissolving both the unexposed resist in the top layer and the bottom release layer. After the particles are removed from the wafers, the particle/developer dispersions are thoroughly washed by repeated centrifugation, decanting, and adding fresh developer. After cleaning, the dispersions are concentrated to a volume fraction ≈ 10^{-4} and mixed with 5CB. To remove the developer from the 5CB solvent, the mixture is placed in a convection oven held at a temperature of 60 °C while under vacuum for 24 h. To disperse colloids in 5CB, the dispersion is agitated using an ultrasonic bath held at a temperature above the nematic–isotropic transition temperature for 1 h. This preparation procedure shows that, similar to regular confining surfaces of LC cells, one can mechanically buff a photoresist film along selective directions and define an anchoring easy axis on either the top or the bottom surface of lithographically fabricated colloidal platelets (Figure 6).

https://doi.org/10.1021/acs.langmuir.2c00611
Langmuir XXXX, XXX, XXX–XXX

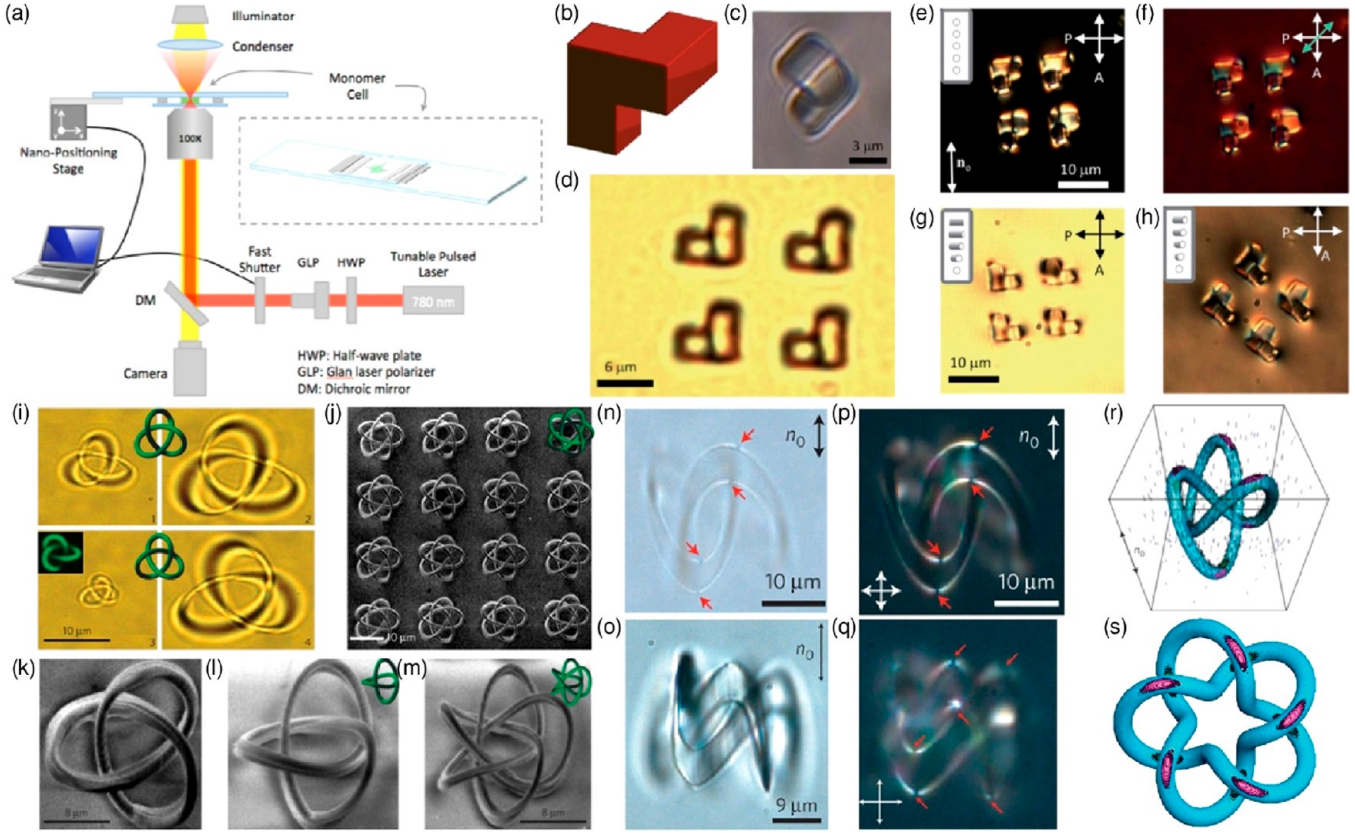

Figure 8. Two-photon polymerization. (a) Schematic diagram of a multiphoton absorption photopolymerization setup. (b) Computer-generated model of a low-symmetry colloidal particle. (c, d) Bright-field optical images of (c) a single particle and (d) an array of four surface-bound particles obtained from the model in b using two-photon polymerization. (e−h) Microscope textures of microparticles in (e, f) planar and (g, h) twisted nematic cells. Adapted with permission from ref 95. Copyright 2012 Royal Society of Chemistry. (i) Optical microscopy textures showing left-handed (panels 1 and 2) and right-handed (panels 3 and 4) trefoil colloidal torus knots $T(3;2)$ of different sizes with corresponding 3D models shown in green. Top-left inset in panel 3 shows a 3PEF-PM image of a colloidal particle. (j) SEM of a 4×4 array of torus knots $T(5;3)$. (k−m) Zoomed-in SEMs of single (k, l) $T(3;2)$ and (m) $T(5;3)$ knots shown from different perspectives along with corresponding 3D models (depicted in green), as viewed (k) along the torus axis and (l, m) in an oblique direction. (n−q) Optical micrographs of (n, p) a trefoil knot particle and (o, q) a $T(5;2)$ knotted particle obtained (n, o) without and (p, q) with crossed polarizers aligned as indicated by white double arrows; boojums visible within optical micrographs are marked by red arrows (n, p, q). (r) Computer-simulated $\mathbf{n}(\mathbf{r})$ at the particle−LC interface (black rods) and in the bulk (blue rods) induced by a trefoil knot particle. Green and magenta areas show a reduced scalar order parameter of 0.42, corresponding, respectively, to $s = -1$ and 1/2 defects at the particle−LC interface. (s) Numerical model showing surface defects induced by the $T(5;2)$ particle as viewed along the torus axis. Adapted with permission from ref 96. Copyright 2014 Springer Nature.

Regular polygonal platelets with planar degenerate anchoring align in distinct ways relative to the far-field alignment $\mathbf{n}_0$ of the LC. For example, polygons with an odd number of sides, such as triangles and pentagons, align with one edge parallel to $\mathbf{n}_0$ and give rise to $\mathbf{n}(\mathbf{r})$-deformations with an elastic dipole moment $\mathbf{p}_{el}$ perpendicular to $\mathbf{n}_0$. Colloidal polygonal prisms having an even number of sides, such as squares, align such that all edges are at 45° to $\mathbf{n}_0$ and result in quadrupolar $\mathbf{n}(\mathbf{r})$ (Figure 6b and 6d). These particular orientational states and accompanying $\mathbf{n}(\mathbf{r})$-configurations arise from minimizing the elastic free energy in the surrounding LC, which are consistent with planar degenerate anchoring of $\mathbf{n}(\mathbf{r})$ on all of their surfaces. By breaking the degeneracy of the planar anchoring at one or more surfaces of a polygonal colloidal object, other orientational states and accompanying $\mathbf{n}(\mathbf{r})$-configurations can be stabilized in a reproducible and controlled fashion (Figure 6c and 6e). The rubbing not only defines a different orientation of the square platelet but also causes an elastic dipole moment $\mathbf{p}_{el}$ that points along a normal to the broken symmetry plane (Figure 6c and 6e), orthogonally to $\mathbf{n}_0$. This different symmetry then controls colloidal self-assembly (Figure 6f and 6g) into dipolar chains orthogonal to $\mathbf{n}_0$.

Direct Laser Writing. A more advanced technique for fabrication of colloidal particles is based on a direct laser writing approach.[90] Direct laser writing is a high-resolution, versatile photolithography method where the local solidification of a photoresist at the focus of a laser beam allows drawing of structures on the nanometer scale.[91] This approach does not need to use expensive masks and photolithography steps in the fabrication process and offers a better resolution and more flexibility in defining the complex shapes of the colloidal particles. Colloids can also be anisotropic, chiral, typically in terms of their shape and topology and chemical functionalization of their surfaces. The direct laser writing method was used for fabrication of a number of colloidal particles with different complex shapes and topologies.[60−62] Fabrication of silica (SiO_2) colloidal particles involves the following procedures. First, a 90 nm sacrificial layer of aluminum is sputtered on a silicon wafer (Figure 7ai and 7ii). Then, a 1 μm silica layer is deposited on the aluminum by plasma-enhanced chemical vapor deposition, and a photoresist AZ5214 is spin-coated on the silica layer (Figure 7aiii and 7iv). The pattern of the particles is defined in the photoresist by illumination at 405 nm with a direct laser writing system and then in the silica layer by inductively coupled plasma etching (Figure 7av and 7vi). Finally, the photoresist is removed with acetone, and the aluminum is wet etched with a sodium hydroxide aqueous solution so that the silica particles are released and then redispersed in deionized water (Figure 7aix). They are washed out by deionized water (3−4 times) to obtain an aqueous dispersion of colloidal particles. Fabrication with direct laser writing can yield up to $\sim 10^8$ highly monodisperse particles on a single wafer. The drawing

https://doi.org/10.1021/acs.langmuir.2c00611
Langmuir XXXX, XXX, XXX−XXX

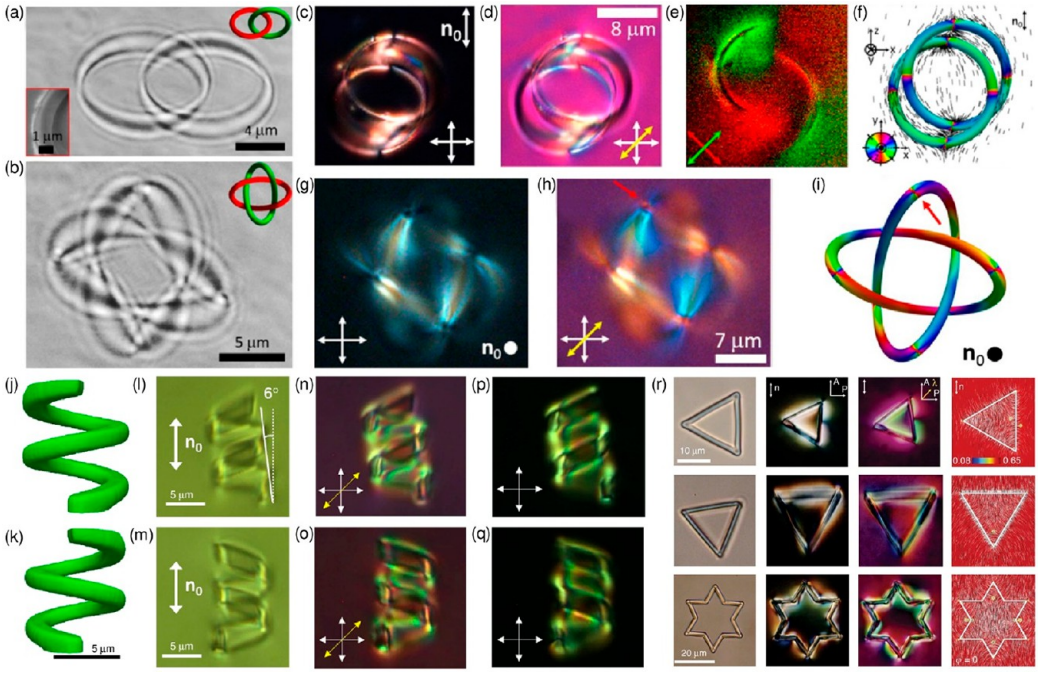

Figure 9. Photopolymerized colloidal links, microsprings, and fractal particles. (a) Optical bright-field micrograph of a Hopf link particle and (upper right inset) the corresponding 3D model. (lower left inset) SEM image of a photopolymerized tube from which all linked particles are made. (b) Bright-field micrograph of a Solomon link particle, and (inset) corresponding 3D model. (c–f) Hopf link particle with tangential anchoring in a nematic LC. (c, d) Polarizing optical micrographs of a colloidal Hopf link in a nematic cell as viewed between crossed polarizers (white double arrows) (c) with and (d) without a retardation plate (yellow double arrow). (e) In-plane cross-sectional composite 3PEF-PM image of a Hopf link and $\mathbf{n}(\mathbf{r})$ around it obtained by superimposing two 3PEF-PM scans (with fluorescence shown in green and red colors) acquired using orthogonal, linear polarizations of excitation light along directions depicted by green and red double arrows. (f) Perspective view of a numerically calculated $\mathbf{n}(\mathbf{r})$ depicted using colors on the particle's surfaces and using rods in the LC bulk. Colors on the surfaces of the particle show azimuthal orientations of $\mathbf{n}(\mathbf{r})$ with respect to $\mathbf{n}_0$ according to a color scheme shown in the lower left inset. (g–i) Colloidal Solomon links with tangential surface boundary conditions in a nematic LC. Adapted with permission from ref 97. Copyright 2015 National Academy of Sciences. (j, k) Right- and left-handed colloidal springs, respectively, imaged with 3PEF-PM while surrounded by an isotropic medium (immersion oil). Optical micrographs of (l, n, p) right- and (m, o, q) left-handed colloidal microsprings in 5CB imaged using bright-field (l, m) and polarizing microscopy without (p, q) and with (n, o) a retardation plate. Adapted with permission from ref 98. Copyright 2018 Springer Nature. (r) Nematic topological states stabilized by fractal Koch-star colloidal particles. Adapted with permission from ref 99. Copyright 2017 Springer Nature.

speed depends on the particles' dimensions and their density on a wafer, and it takes about 5–10 min to draw microparticles within a 1 × 1 cm^2 region.[60] To promote perpendicular boundary conditions for $\mathbf{n}(\mathbf{r})$ on the surface of particles, they can be treated with an aqueous solution (0.05 wt %) of DMOAP and then redispersed in methanol. This dispersion can be then mixed with 5CB to obtain a nematic dispersion after methanol evaporation overnight at an elevated temperature of 70 °C.

Using direct laser writing, a number of colloidal particles of different geometrical and topological complexities were fabricated.[60−62,92] Topological colloids with a genus $g = 1–5$ with homeotropic anchoring in nematic LCs[60] (Figure 7b–h) induce 3D director fields $\mathbf{n}(\mathbf{r})$ and topological defects dictated by the colloidal topology and spontaneously align with their ring planes either perpendicular or parallel to $\mathbf{n}_0$, depending on the interplay between the LC elastic and surface-anchoring forces as well as on the dimensions of the topological colloids with respect to the thickness of the experimental cells.[60] Fabrication of these handlebody particles allowed to show experimentally that topological charge is conserved and that the total charge of particle-induced defects always obeys predictions of the Gauss–Bonnet and Poincaré–Hopf index theorems for colloids with topology distinct from the topology of a sphere.[60,92] Colloidal particles fabricated in the shape of truncated flat pyramids (Figure 7j–o) with homeotropic surface anchoring orient with their large faces normal to $\mathbf{n}_0$, giving a rise to peculiar $\mathbf{n}(\mathbf{r})$-distortions determining LC-mediated elastic interactions between colloids and their self-assembly.[61,93] Spiral particles (Figure 7p and 7q) with homeotropic or tangential anchoring can cause chiral symmetry breaking of elastic distortions in a host nematic.[62]

Two-Photon Polymerization. The two-photon polymerization technique has another advantage over previously described methods by allowing the fabrication of fully 3D colloidal particles of complex topology at micro- and nanoscales.[90] Anisotropic colloidal particles were essential in recent efforts to reproduce the complexity of atomic bonding in self-assembled colloidal structures.[94] However, all anisotropic colloids fabricated using photolithography or direct laser writing techniques exhibit relatively high symmetry, and fabricated colloids typically offer limited variations of surface topology.[60] To obtain the rigid colloidal particles of especially complex shape and topology, the two-photon photopolymerization method can be used.[95−97] A schematic diagram of a two-photon photopolymerization setup is shown in Figure 8a, where a tunable femtosecond laser is used as an excitation light source. A femtosecond laser beam, for example,[95] at 780 nm is introduced into an inverted microscope and focused into a sample by an oil-immersion 100× objective with a high numerical aperture NA = 1.4. The nonlinear nature of the multiphoton-absorption-based photoinitiation process causes polymerization to occur only in the vicinity of the focused beam's focal point with the subdiffraction-limited resolution dependent on the used laser power. Commercial or LabView-based homemade computer software can be used for synchronous control of both the shutter and the nano-positioning stage to polymerize arbitrary 3D topological colloids. The exposure of the sample is controlled by a fast shutter introduced into the optical train of the photopolymerization setup before the microscope (Figure 8a). During the photopolymerization, a computer-controlled *XYZ* nanopositioning stage changes the relative 3D position of the sample with respect to the focal point of the focused femtosecond laser

https://doi.org/10.1021/acs.langmuir.2c00611
Langmuir XXXX, XXX, XXX−XXX

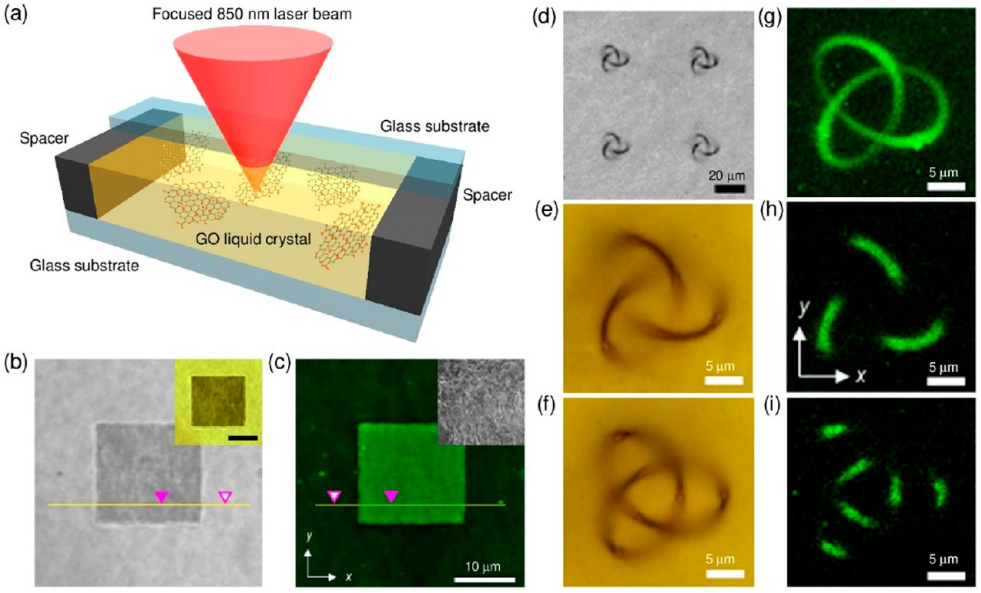

Figure 10. Topologically nontrivial rGO structures in a bulk of an aqueous GO flakes dispersion. (a) Schematic diagram of rGO particles fabrication. (b) Transmission-mode optical micrograph of a freely suspended rGO plane particle (a dark square) in an aqueous dispersion of GO flakes obtained using 850 nm laser light; (inset) same sample area obtained using visible white light. (c) Photoluminescence texture of the rGO plane (a bright square) shown in b; (inset) $6 \times 6\ \mu m^2$ SEM image of a surface of a rGO plane microparticle. (d) Optical bright-field micrograph of an array of rGO trefoil knots. (e, f) Optical bright-field microscopy textures of an rGO left-handed trefoil knot focused on the (f) middle and (e) top of the knot. (h, i) Photoluminescence micrographs of an rGO trefoil knot scanned in the (i) middle and (h) top planes of the knot. (g) 3D perspective view of an rGO left-handed knot reconstructed from photoluminescence data. Adapted with permission from ref 103. Copyright 2015 Springer Nature.

beam with a high precision on the order of subnanometers. The intensity of the laser beam and its polarization at the sample plane can be controlled by a pair of a Glan laser polarizer and a half-wave plate. To imprint a computer-generated 3D shape into the photocurable material, the *XYZ* stage is continuously translated and the shutter is timed so that the focus of the femtosecond laser beam can visit and sequentially polymerize all points of the desired volume of the complex-shaped colloidal microparticle.

The experimental cells used for the photopolymerization typically consist of two glass coverslips spaced with film spacers, and one of coverslips is spin coated with a thin film of unidirectionally rubbed poly(vinyl alcohol) (PVA) or other aligning agent. A small drop of UV-curable optical adhesive NOA-61 (Norland Inc.) is sandwiched between two coverslips held together by, for example, two pieces of Scotch tape. Next, the cell is placed on a mounting clip attached to the *XYZ* stage, so that it can be scanned over the objective during the photopolymerization of 3D colloidal particles within the drop of optical adhesive (inset of Figure 8a). During this process, the polymerization starts at the interface with PVA and then advances away from the substrate with PVA as the sample is shifted along the microscope's optical axis to "draw" the consecutive layers of a colloidal particle. Obtained particles can be kept surface bound or released from the substrate by carefully poking with a needle under the optical microscope and then suspended within the LC. Similar particles can be also polymerized in other materials, such as NOA-63 (Norland Inc.), IP-G (NanoScribe GmbH), and the ultraviolet-sensitive photopolymer SU-8 commonly used in photolithography. In the last two cases, the particles could be photopolymerized in the bulk of the cell, so that no mechanical or chemical detachment from the surfaces is needed.

The polymerized IP-L photoresist induces strong tangentially degenerate anchoring at the interface between the polymer and the nematic LCs such as 5CB or others. Therefore, as-prepared particles from IP-L photoresist impose tangential boundary conditions at their surfaces. One can also achieve homeotropic anchoring when using mixtures containing 75−98 wt % IP-L photoresist and 2−25 wt % styrylethyltrimethoxysilane. After rinsing the polymerized structures as described above, they should be submerged in a 0.5 wt % solution of DMOAP in isopropanol for several minutes to allow bonding between the silane chemical moieties in DMOAP and those exposed on the surface of the polymerized mixture. They are then rinsed again with isopropanol before being detached from the surface for retrieval and mixing with the LC. Alternatively, to achieve homeotropic anchoring, instead of doping IP-L with styrylethyltrimethoxysilane, plasma treatment (for about 5 min) also can be used on the photopolymerized colloids composed of IP-L without additives followed by surface modification with DMOAP using a procedure similar to that described above.

Two-photon polymerization allows for the fabrication of structures and particles attached to surfaces[95] as well as free-standing[96,98,99] and interconnected[96] particles. Three-dimensional surface-bound particles with tangential surface anchoring (Figure 8b−h) were designed[95] using two-photon polymerization, demonstrating that they can cause low-symmetry, long-range elastic $\mathbf{n}(\mathbf{r})$-distortions, induce twist of the director, and impose elastic torque on the nematic LC $\mathbf{n}(\mathbf{r})$ which is transmitted on large distances. Such particles may enable creative means of patterning bulk alignment of nematic LCs and the design of long-range elastic interactions between the nematic LC fluid-borne and surface-attached colloidal particles for their structured elasticity-mediated self-assembly.

Two-photon polymerization was also used to fabricate especially complex colloidal particles with the surface topology of torus knots $T(p,q)$.[100,101] These particles are formed by knotted polymeric rigid tubes that, before having their ends joined, are looped p times through the hole of an imaginary torus with q revolutions about the torus rotational symmetry axis (Figure 8i−s). Colloidal knots with tangential surface boundary conditions distort $\mathbf{n}(\mathbf{r})$, which approaches the uniform $\mathbf{n}_0$ at large distances from the particles, but because their complex shape is incompatible with the homogeneous field of the aligned nematic LC, boojums emerge at the surfaces of colloidal particles and, due to scattering, are visible in bright-field micrographs as dark points (Figure 8n−q).

Using this method, colloidal microparticles with differently linked components were also realized.[97] They are shaped as closed solid polymeric rings with disconnected surfaces that both freely move relative to each other (Figure 9a−i). After dispersing in a nematic LC, these particles induce a large variety of $\mathbf{n}(\mathbf{r})$-configurations and looped

https://doi.org/10.1021/acs.langmuir.2c00611
Langmuir XXXX, XXX, XXX−XXX

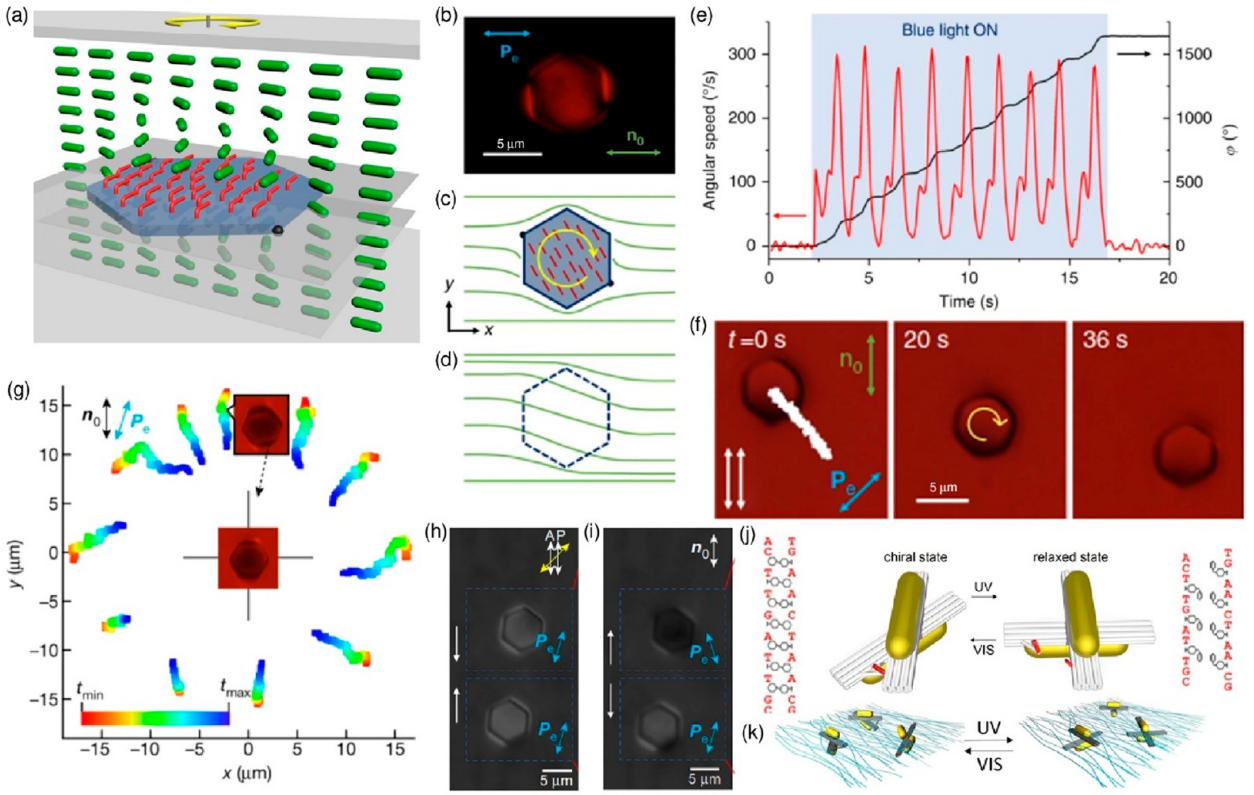

Figure 11. (a) Schematic of a self-assembled molecular-platelet motor suspended in a nematic LC between two confining glasses. Green rods represent $\mathbf{n}(\mathbf{r})$; red rods show azobenzene molecules on the platelet surface; black semisphere on one of the vertices of the hexagon represents boojums; circular yellow arrow shows direction of rotation. (b) Polarizing micrograph obtained with red imaging light when a platelet is illuminated by linearly polarized blue light with $\mathbf{P}_e \| \mathbf{n}_0$. (c, d) Corresponding schematics of $\mathbf{n}(\mathbf{r})$ (green lines) (c) in the plane of platelets and (d) beneath the platelet. (e) Time dependence of spinning angular speed and a net azimuthal rotation angle φ of a colloidal motor probed in the presence and absence of blue light. (f) Video frames of translational motion of about 1 μm thick colloidal platelets accompanied by its rotation (yellow circular arrows) under blue light with polarization $\mathbf{P}_e$ at 45° relative to $\mathbf{n}_0$. Elapsed time is marked on images. Adapted with permission from ref 107. Copyright 2018 Springer Nature. (g) Colloidal attractions of two monopoles with same signs at all orientations manifested by color-coded trajectories, where $\mathbf{P}_e$ is at about 20° with respect to $\mathbf{n}_0$. (Insets) Micrographs of the interacting particles, and black dashed arrow indicates the direction of relative motion. (h, i) Polarizing micrographs of elastic monopoles with same/opposite sign by exposing to linearly polarized blue light with same/opposite polarization. Pair of white arrows indicates attraction/repulsion of two monopoles. Adapted with permission from ref 115. Copyright 2019 Springer Nature. (j) Photoswitching on chiral and nonchiral states of gold nanorods templated by DNA origami. Given the trans−cis isomerization of azobenzene, the DNA origami undergoes hybridization and dehybridization on ultraviolet and visible light illumination. (k) Schematic of photoswitching chirality of plasmonic origami in a cellulose nanofiber-based nematic LC. Adapted with permission from ref 26. Copyright 2019 Optical Society.

and linked vortex lines that entangle the linked components of colloidal particles, resulting in their elastic coupling. Linked colloidal rings can induce $\mathbf{n}(\mathbf{r})$-configurations, which are topologically distinct from each other but always satisfy the topological constraints. Chiral spring-like colloidal particles of different handedness and with tangential boundary conditions (Figure 9j−q) were fabricated using two-photon polymerization to study the effects of chirality on the director structures and LC-mediated elastic interactions between chiral particles.[98] To study coupling between the fractal order and the uniaxial nematic vector-type ordering, polymer Koch-shaped hollow colloidal prisms of three successive fractal iterations were produced by two-photo polymerization,[99] and their surfaces were treated with DMOAP silane to create a homeotropic surface alignment of LC molecules (Figure 9r).

Preparation of Colloidal Microparticles through Controlled Aggregation of Graphene Oxide Flakes. There is high and still growing interest in carbon-based materials such as carbon nanotubes, graphene nanosheets due to their outstanding physical, chemical, thermal, and electric properties.[102] Carbon-based materials can offer the possibility to obtain colloidal particles with the electrical properties of dielectrics, semiconductors, and conductors. The two-photon polymerization method and setup can be also used for three-dimensional patterning of solid microstructures and colloidal particles from reduced graphene oxide (rGO) using laser reduction of colloidal graphene oxide (GO) in LC dispersions.[103] Fabrication of rGO solid colloids starts from the preparation of aqueous dispersions of GO flakes. The improved, mostly single-layer GO flakes were synthesized by methods[104] modified for their large-scale production and obtained as a dispersion in deionized water.

To prepare a sample for three-dimensional patterning with a two-photon polymerization, the aqueous dispersion of GO flakes was first tip sonicated for a few hours at about 35 W of ultrasonic power using a sonifier operating at 20 kHz, which allows one to obtain monodisperse flakes of smaller size.[105] Higher concentrations of GO flakes in dispersions allow for obtaining a homogeneous nematic LC phase. LC dispersions of GO are sandwiched between two clean untreated glass substrates for laser-induced reduction of GO flakes. A gap between substrates can be set using Mylar films of desired thickness. Dispersions of GO flakes should be sonicated in an ultrasonic bath for several minutes before assembling a cell to remove preexisting aggregates. Evaporation of water from the experimental cells can be prevented by sealing samples with an ultraviolet-curable glue NOA-63.

The integrated 3D laser-induced reduction of aqueous GO flake samples can be performed at room temperature using the same two-photon polymerization setup as shown in Figure 8a. The excitation beam is directed to the sample by a system of mirrors and focused into the sample (Figure 10a) using a high numerical aperture oil objective. The spatial 3D position of the excitation beam in the volume of the

https://doi.org/10.1021/acs.langmuir.2c00611
Langmuir XXXX, XXX, XXX−XXX

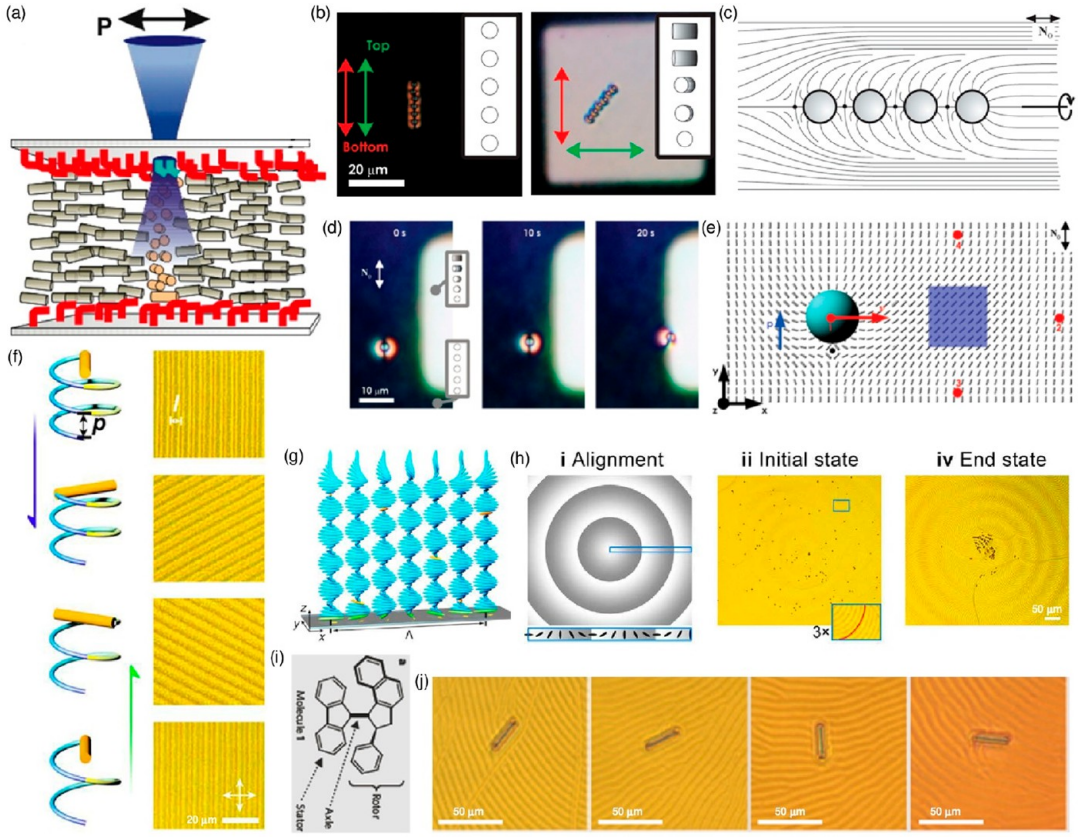

Figure 12. (a) Schematic of the light-controlled orientation of LC molecules via azobenzene monolayers (red rod) bounded on the glass surface. (b) Rotation of a self-assembled chain of dipolar silica spheres within a light-reconfigurable twisted domain. Chain of dipolar spheres rotates by one-half of the twisted angle. (c) Director field $\mathbf{n}(\mathbf{r})$ around the chain of dipolar spheres. (d) Snapshots of a dipolar colloid interacting attractively to a twist domain; elapsed time is marked on images. (e) Simulated $\mathbf{n}(\mathbf{r})$ in the midplane of a cell with a dipolar particle and an $\pi/2$ twist domain (blue); elastic dipole moment $\mathbf{p}$ and velocity v are marked, respectively, by blue and red arrows. Adapted with permission from ref 106. Copyright 2011 National Academy of Sciences. (f) Schematic of unwinding/winding of cholesteric LC helixes (left) under blue/green light illumination and corresponding grating cholesteric LC textures (right). Orange cylinders denote the directions of grating stripes. White double arrows the orientation of crossed polarizer is given with double white arrows. (g) Helical configuration of the photopatterned cholesteric LC film with green rod represents an azobenzene molecule, and blue rod denotes LC molecule. (h) Converging of numerous microspheres took place on a radial periodic aligning cholesteric LC film with alignment condition (left), initial state (middle), and end state (right) given. Adapted with permission from ref 108. Copyright 2021 American Association for the Advancement of Science. (i) Structure of a molecular motor. (j) Rotation of a glass rod placed on a LC film upon irradiation with ultraviolet light. Adapted with permission from ref 109. Copyright 2006 Springer Nature.

sample can be controlled, for example, with the galvanomirror scanning unit. The 3D reduction of aqueous GO flakes is performed using a pulsed laser beam at 850 nm and a moderate laser fluence. The dwell time or scanning speed is also controlled by a scanning unit. The fabricated solid rGO colloidal particles can be imaged using the same setup with an average laser power for photoluminescence imaging (Figure 10c and 10g−i) low enough to prevent the photo and thermal damage. For this, excitation of the GO flakes is performed also at 850 nm, and the unpolarized photoluminescence light can be detected in a range of about 400−700 nm in a backward mode with a photomultiplier tube detector (Figure 10c and 10g−i). The polarization of excitation could be varied using phase retardation plates mounted before an objective.

Photoresponsive Surface Interactions as Means of Controlling Nematic Colloids. Surface interactions on colloidal particles' surface allow for the activation of their translational or rotational motion due to facile response to light[106−110] or other external stimuli.[111,112] Among the key features allowing the transformation of passive colloidal inclusions into micromotors and micromachines are functionalization of azobenzene dye molecules on the surface of colloidal particles[105,113−115] or using azobenzene dyes in the anisotropic nematic fluid host.[106,100−108,116−123]

When it comes to designing and synthesizing azobenzene dye to be functionalized on the particle surface, one needs to keep in mind that the azobenzene dye should be robustly attached onto the surface and needs to readily respond to light within a viscous nematic medium. In our works,[106,107] for example, derivatized methyl red (dMR) is synthesized and coated onto the particle's surface in a single, covalently bound layer.[124] The dMR monolayer exhibits high sensitivity to blue and ultraviolet light, which gives rise to efficient energy transduction in a light-driven motor.[107] The representative colloidal micromotors are formed by thin, optically transparent silica platelets fabricated via direct laser writing photolithography[60] with monolayers of dMR molecules self-assembled on their surfaces (Figure 11a). To promote surface binding of dMR molecules, platelets are immersed in a piranha solution for about 1 h to produce hydroxylated colloidal surfaces. Then, they are submerged in 20 mL of a toluene solution containing 5 mg of dMR and 20 μL of *n*-butylamine and kept overnight at an elevated temperature of 45 °C, followed by rinsing with toluene and curing at 120 °C for 2 h. The resulting platelets are then dispersed in isopropanol and can be mixed with a nematic LC. Isopropanol should be evaporated (for example, at 75 °C, above the nematic−isotropic transition temperature) after mixing with the LC and forming the LC colloidal dispersion (Figure 11a).

In the presence of blue excitation light with polarization $\mathbf{P}_e$, which is different from that perpendicular to $\mathbf{n}_0$ (Figure 11d), the azobenzene moieties anchored on the platelet surface rotate to orient orthogonal to $\mathbf{P}_e$, causing $\mathbf{n}(\mathbf{r})$ to twist above and beneath the platelet (Figure 11a),

https://doi.org/10.1021/acs.langmuir.2c00611
Langmuir XXXX, XXX, XXX−XXX

which, in turn, rotates $\mathbf{n}(\mathbf{r})$ at the platelet−LC interfaces together with the platelet itself (Figure 11b−d). The twist configuration within the LC layer above a platelet again modifies the polarization state of light traversing the platelet, thus promoting additional rotation of azobenzene moieties, the platelet, and $\mathbf{n}(\mathbf{r})$ to yield an opto-mechanical cycle. The rotation angular speed exhibits apparent periodicity (Figure 11e). For thick ≥ 1 μm platelets, the optical response of azobenzene at the edge faces additionally breaks the symmetry of director distortions, which can result in the conversion of rotation into translation (Figure 11f). Translation of colloidal particles can also be prompted by the continuous trans−cis−trans isomerization of azobenzene attached on the particle surface, where the trans−cis−trans isomerization generates a microsized isotropic phase inducing an elastic force between nematic and isotropic phases to drive particles.[114]

The rotation direction of colloidal platelet can be predefined by slightly deviating the light polarization $\mathbf{P}_e$ away from $\mathbf{n}_0$, in which perturbations of $\mathbf{n}(\mathbf{r})$ are monopole like (Figure 11c) and the elastic charge of the monopole has the same sign as θ (θ is the angle between $\mathbf{P}_e$ and $\mathbf{n}_0$). The sign of their monopole moments can be switched by rotating the linear polarization of light in an opposite direction (Figure 11h and 11i). However, unlike in electrostatics, like-charged elastic monopoles with the same signs attract (Figure 11g and 11h), while oppositely charged ones repel each other (Figure 11i). This happens due to the tendency of the LC to minimize the distortions of $\mathbf{n}(\mathbf{r})$, where like-charged elastic monopoles (with a similar direction of director rotation around them) can reduce created elastic distortions when spatially approached, whereas oppositely charged monopoles can only minimize the free energy by increasing their distance.[115] By optically switching the direction of the particle's rotation and the colloidal monopole's sign, this system allows for fascinating switching of colloidal interactions between repulsive and attractive with light.

Azobenzene molecules as incorporated into big molecules, such as DNA strands, can also help to photoswitch the chirality of DNA origami-templated plasmonic nanomaterials.[116] For example, the azobenzene molecules are in the trans form when exposed to visible light, causing hybridization of the DNA origami, which endows the composite chiral state with gold nanorods attached to the DNA origami and dispersed in the cellulose nanofiber nematic medium (Figure 11j and 11k). In contrast, on ultraviolet light illumination, the azobenzene molecules switch to the cis form, resulting in dehybridization of the DNA origami and an achiral form of the nanomaterial, as demonstrated in ref 116. This, in turn, allows for optical control of mesoscale composites based on plasmonic nanoparticles scaffolded by colloidal origami within lyotropic nematic LC host media.[116]

Manipulation of colloidal particles in nematic host can also be accomplished by means of bonding a light-controlled dMR monolayer on the inner glass surfaces of the LC cells.[106] To obtain a monolayer on the confining glass plates, these glass plates are typically cleaned by immersing in a piranha solution for 1 h, rinsing with isopropanol, and curing at 100 °C for 1 h. The cleaned glass plates are then soaked in dMR solution (1 wt % in toluene) for 90 min at 45 °C to facilitate surface bonding of dMR molecules, which is followed by a toluene rinse to wash away the excess dMR, dry nitrogen blowing, and curing for 2 h at 115 °C. The cell then is fabricated by assembling two glass plates with a gap defined by the size of the silicon spacers. The boundary conditions at the top and bottom surfaces can be independently controlled; therefore, a domain with designable twist angle across the cell can be generated (Figure 12a and 12b). In such twisting director field landscape, particles, and their self-assembled structures, such as chains of dipolar colloids (Figure 12c), rotate their directions and follow the twist orientation of $\mathbf{n}(\mathbf{r})$ in the cell midplane. The light-induced $\mathbf{n}(\mathbf{r})$ twisted domain also exerted anisotropic interactions to colloids with strong boundary conditions. For example, a particle with a dipolar $\mathbf{n}(\mathbf{r})$ structure interacts attractively with the twisted domain (Figure 12d) in order to eliminate the energetically costly region of strong elastic distortions between the particle and the trap (Figure 12e). In contrast, colloidal particles with the same orientation of the elastic dipole moment $\mathbf{p}$ in position 2 experience repulsion (Figure 12e).

With azobenzene film on the inner confining glass surfaces, additional functionalized dopant in the LC host, e.g., photosensitive chiral dopant, or with additional employment of an electric field, external stimuli can effectively promote microparticle motions in a customized way.[108,110] For example, when a photoresponsive left-handed chiral dopant is adopted, the semifree cholesteric LC film (Figure 12g, with only one confining substrate) undergoes reversible unwinding/winding upon exposure to blue/green light due to the change of chiral dopant conformation (Figure 12f).[108] The unwinding of the cholesteric LC layer causes synchronous rotation of the grating texture (Figure 12f), and the rotation then leads to a translation of sputtered microparticles. By making use of this feature, Ma et al.[108] demonstrated collective convergence (Figure 12h), divergence, aggregation, and orbiting of numerous microspheres within the LC film. Similarly, doping helical molecules featuring photoreconfigurable chirality allowed for rotating microparticles within a LC film.[109] In the presence of ultraviolet light, isomerization occurs around the central double bond (Figure 12i), which results in cholesteric's handedness inversion from left- to right-handed. A subsequent thermal step again causes a helicity switch from right- to left-handed at 20 °C, and so on. Interestingly, the helicity inversion accompanies reorganization of the grating texture of a cholesteric LC film in a rotational fashion and leads to the rotation of microparticles sprinkled on the LC film (Figure 12j).

The defect structure induced by the immersed colloidal droplets can be tailored by azobenzene doped in a LC host.[116−123] The trans−cis isomerization of azobenzene upon exposure to ultraviolet light causes the surface boundary condition of the glycerol droplets to switch from homeotropic to tangential alignment. As a result, the topological defect structure of the Saturn ring around the droplets transforms into that containing two boojums. The opposite structural transformation from two boojums to a Saturn ring can then take place under visible light irradiation accompanying cis−trans isomerization.[116−121]

CONCLUSION

The above overview of methodologies developed for fabricating various nematic LC colloids shows that the colloidal particles can be predesigned to induce desired director distortions and topological defects in the LC host media.[125−152] This allows for designing and realizing colloidal analogs of atoms that can interact in well-defined ways, for example, mimicking interactions of multipolar charge distributions ranging from monopoles to hexadecapoles and even higher order multipoles.[8,25,70] Compared to electrostatics however, these interactions are further enriched by the LC's elastic constant anisotropy, the more complex nature of multipolar director field configurations as compared to (scalar in nature) multipolar charge distributions in electrostatics, as well as the large variety of emergent effects related to the near-field interactions, topological defects, screening of distortions due to finite-size effects, and confinement, etc. The electrostatics analogy, however, provides the initial set of considerations for designing interactions and self-assembly of nematic colloids.[5,8,17,25,52−58,150] External stimuli, such as light and electric or magnetic fields, can be used to reconfigure interactions between the nematic colloids, including the very possibility of turning attractive interactions into repulsive interactions and vice versa.[115] The use of electrostatic interactions enabled by the colloidal particle's surface charging[63,64] allows for counterbalancing the anisotropic (including strongly attractive) forces arising due to the orientational elasticity of LCs with the (Coulomb-like) electrostatic repulsive interactions, which helps to eliminate the issue of too strong binding (thousands of k_BT) between nematic colloidal objects that cannot be overcome by the strength of thermal fluctuations.[78−82] Thus, LC host media provide a versatile platform for controlling both the anisotropy and the strength of the interparticle forces, which is essential for controlling their self-assembly. This approach already helped to realize molecular−colloidal analogs of orthorhombic and

https://doi.org/10.1021/acs.langmuir.2c00611
Langmuir XXXX, XXX, XXX−XXX

monoclinic biaxial nematic fluids, ferromagnetic (chiral) nematic LC colloids, triclinic and other colloidal crystals, and so on.

Nematic LC colloids also display fascinating diversity of the particle-induced defects,[60,132−134] which can take geometries and topologies ranging from point and line and surface defects, where the lines can take the forms of closed loops corresponding to unknots (rings) or various torus knots. Furthermore, the closed loops can be linked (or not) with knotted particles and other defect loops.[96−98] Like in the case of multipolar distributions, the structure of the particle-induced defects can be reconfigured by external stimuli like fields and light. Beyond the self-assembly arising from the long-range interactions due to the elastic field deformations induced by the particles, the nematic colloidal particles can self-assemble through sharing or interlinking of defect lines.

While the majority of studies of nematic colloids focused on equilibrium conditions, these systems display even more fascinating types of behavior when they are driven out of equilibrium. The phenomena reported so far include various types of colloidal translations and rotations,[75,107,125,136] with the motions arising due to nonreciprocal dynamics of the director field distortions around particles, backflow, various electrophoretic and dielectrophoretic effects, etc. The motion directions as well as spinning and orbiting behaviors can be controlled using particles with desired shapes, symmetry breaking due to particle-induced defects, deposited layers of metal, etc.

While 25 years[4,5] of intensive research on nematic colloids has brought about many emergent effects and novel types of physical behavior, the research so far has mainly focused on understanding of the vast variety of physical behaviors in such systems. At the same time, these systems could allow for the "inverse design" of the physical behavior like self-assembly and tailored interactions by designing particles and conditions under which they interact and self-assemble. Past studies provided a solid platform to pursue such efforts, but very little has been done so far in this direction. By designing interparticle interactions between colloidal objects with different shapes, topologies, and chemical compositions, hypothetically, artificial, man-made materials of desired properties can be realized through mesoscale colloidal self-assembly.[78,79,81] The self-assembly-based approaches to fabricate new materials by design is perhaps the most promising research direction in the liquid crystal, colloidal, and overall soft matter research fields.

AUTHOR INFORMATION

Corresponding Author

Ivan I. Smalyukh − *Department of Physics, Department of Electrical, Computer and Energy Engineering, Soft Materials Research Center and Materials Science and Engineering Program, and Chemical Physics Program, Departments of Chemistry and Physics, University of Colorado, Boulder, Colorado 80309, United States; Renewable and Sustainable Energy Institute, National Renewable Energy Laboratory and University of Colorado, Boulder, Colorado 80309, United States;* orcid.org/0000-0003-3444-1966; Email: ivan.smalyukh@colorado.edu

Authors

Bohdan Senyuk − *Department of Physics, University of Colorado, Boulder, Colorado 80309, United States*

Cuiling Meng − *Department of Physics, University of Colorado, Boulder, Colorado 80309, United States*

Complete contact information is available at: https://pubs.acs.org/10.1021/acs.langmuir.2c00611

Author Contributions

The manuscript was written through contributions of all authors, who have given approval to the final version of the manuscript.

Notes

The authors declare no competing financial interest.

Biographies

Bohdan Senyuk studied physics, engineering, and materials science at Lviv Polytechnic National University, completing his B.S. degree in 1994 and M.S. degree in 1995. He received his Ph.D. degree in Chemical Physics from Kent State University in 2010. He joined the Department of Physics of the University of Colorado at Boulder as a research associate in 2011. For a period of time in 2011 he also was a postdoctoral research associate at Rice University. His research interests include soft matter, liquid crystals, colloids, and microscopy.

Cuiling Meng received her B.S. and M.S. degrees from the Physics Department at Harbin Institute of Technology in 2013 and 2015, respectively. She then received her Ph.D. degree from the Department of Electronic and Computer Engineering at the Hong Kong University of Science and Technology, Hong Kong, China, in 2019. After that, she started her postdoctoral work at the University of Colorado at Boulder (2020). Her research interests include mesostructured soft matter, novel photoresponsive alignment materials, micromotors, as well as liquid crystal scattering films.

https://doi.org/10.1021/acs.langmuir.2c00611
Langmuir XXXX, XXX, XXX−XXX

Ivan I. Smalyukh obtained B.S. and M.S. degrees from Lviv Polytechnic National University (1995) and Ph.D. degree from Kent State University (2003). He was a postdoctoral research associate at the University of Illinois Urbana−Champaign. He joined the Department of Physics at University of Colorado at Boulder as an Assistant Professor in 2007 and was promoted to Associate Professor in 2014 and Full Professor in 2017. He is a fellow of the Renewable Sustainable Energy Institute and Materials Science Engineering Program and directs the Soft Matter Physics Group at University of Colorado at Boulder. His research focuses on soft matter and biological systems, including liquid crystals, colloids, polymers, bacteria, gels, and biomaterials and their photonic, electro-optic, and energy-related applications. He is a fellow of the American Physical Society. He has received many awards, including the Bessel and Glenn Brown Awards, the PECASE Award from the White House, the GSoft Award from the American Physical Society, and the Langmuir Award of the American Chemical Society.

■ ACKNOWLEDGMENTS

The authors acknowledge the financial support of the research on LC colloids (the U.S. Department of Energy, Office of Basic Energy Sciences, Division of Materials Sciences and Engineering, under Award ER46921, contract DE-SC0019293 with the University of Colorado at Boulder), examples of which have been highlighted within this review. I.I.S. thanks his students and postdocs at the University of Colorado at Boulder who have been working on research topics related to this review, including P. J. Ackerman, H. Mundoor, A. J. Hess, H. R. O. Sohn, J.-S. B. Tai, J.-S. Wu, J. Brewer, Z. Chen, J. S. Evans, M. G. Campbell, C. D. Liu, Q. Liu, A. Martinez, H. C. Mireles, Y. Yuan, Y. Wang, A. J. Funk, M. J. Laviada, I. Klevets, C. Lapointe, J. Giller, S. Park, O. Puls, D. Glugla, M. C. M. Varney, Q. Zhang, M. B. Pandey, R. P. Trivedi, N. P. Garido, R. Visvanathan, and O. Trushkevych. I.I.S. also acknowledges the hospitality of the Tel Aviv University, Israel, where he was partially working on this review during an extended stay.

■ ABBREVIATIONS

LC, liquid crystal; NA, numerical aperture; FCPM, fluorescence confocal polarizing microscopy; 3PEF-PM, three-photon excitation fluorescence polarizing microscopy; SDS, sodium dodecyl sulfate

■ REFERENCES

(1) Chaikin, P. M.; Lubensky, T. C. *Principles of Condensed Matter Physics*; Cambridge University Press: Cambridge, 2000.
(2) de Gennes, P. G.; Prost, J. *The Physics of Liquid Crystals*; Clarendon: Oxford, 1995.
(3) In *Liquid Crystals: Applications and Uses*; Bahadur, B. Ed.; World Scientific: Singapore, 1990; Vol. *1*.
(4) Poulin, P.; Stark, H.; Lubensky, T.; Weitz, D. Novel Colloidal Interactions in Anisotropic Fluids. *Science* **1997**, *275*, 1770−1773.
(5) Poulin, P.; Weitz, D. A. Inverted and Multiple Nematic Emulsions. *Phys. Rev. E* **1998**, *57*, 626−637.
(6) Loudet, J.-C.; Barois, P.; Poulin, P. Colloidal Ordering from Phase Separation in a Liquid Crystalline Continuous Phase. *Nature* **2000**, *407*, 611.
(7) Gu, Y.; Abbott, N. L. Observation of Saturn-Ring Defects around Solid Microspheres in Nematic Liquid Crystals. *Phys. Rev. Lett.* **2000**, *85*, 4719−22.
(8) Stark, H. Physics of Colloidal Dispersions in Nematic Liquid Crystals. *Phys. Rep.* **2001**, *351*, 387−474.
(9) Loudet, J. C.; Poulin, P. Application of an Electric Field to Colloidal Particles Suspended in a Liquid-Crystal Solvent. *Phys. Rev. Lett.* **2001**, *87*, 165503.
(10) Nazarenko, V. G.; Nych, A. B.; Lev, B. I. Crystal Structure in Nematic Emulsion. *Phys. Rev. Lett.* **2001**, *87*, 075504.
(11) Smalyukh, I. I.; Shiyanovskii, S. V.; Lavrentovich, O. D. Three-Dimensional Imaging of Orientational Order by Fluorescence Confocal Polarizing Microscopy. *Chem. Phys. Lett.* **2001**, *336*, 88.
(12) Loudet, J. C. Colloidal Inclusions in Liquid Crystals: Phase Separation Mechanisms and Some Dynamical Aspects. *Liq. Cryst. Today* **2005**, *14* (1), 1−14.
(13) Noël, C. M.; Bossis, G.; Chaze, A.-M.; Giulieri, F.; Lacis, S. Measurement of Elastic Forces between Iron Colloidal Particles in a Nematic Liquid Crystal. *Phys. Rev. Lett.* **2006**, *96*, 217801.
(14) Takahashi, K.; Ichikawa, M.; Kimura, Y. Force between Colloidal Particles in a Nematic Liquid Crystal Studied by Optical Tweezers. *Phys. Rev. E* **2008**, *77*, 020703.
(15) Takahashi, K.; Ichikawa, M.; Kimura, Y. Direct Measurement of Force between Colloidal Particles in a Nematic Liquid Crystal. *J. Phys.: Condens. Matter* **2008**, *20*, 075106.
(16) Kishita, T.; Takahashi, K.; Ichikawa, M.; Fukuda, J.; Kimura, Y. Arrangement Dependence of Interparticle Force in Nematic Colloids. *Phys. Rev. E* **2010**, *81*, 010701.
(17) Pergamenshchik, V. M.; Uzunova, V. A. Dipolar Colloids in Nematostatics: Tensorial Structure, Symmetry, Different Types, and their Interaction. *Phys. Rev. E* **2011**, *83*, 021701.
(18) Chernyshuk, S. B.; Lev, B. I. Theory of Elastic Interaction of Colloidal Particles in Nematic Liquid Crystals Near One Wall and in the Nematic Cell. *Phys. Rev. E* **2011**, *84*, 011707.
(19) Senyuk, B.; Smalyukh, I. I. Elastic Interactions Between Colloidal Microspheres and Elongated Convex and Concave Nanoprisms in Nematic Liquid Crystals. *Soft Matter* **2012**, *8*, 8729.
(20) Gvozdovskyy, I.; Jampani, V. S. R.; Škarabot, M.; Muševič, I. Light-Induced Rewiring and Winding of Saturn Ring Defects in Photosensitive Chiral Nematic Colloids. *Eur. Phys. J. E: Soft Matter Biol. Phys.* **2013**, *36*, 97.
(21) Evans, J. S.; Sun, Y.; Senyuk, B.; Keller, P.; Pergamenshchik, V. M.; Lee, T.; Smalyukh, I. I. Active Shape-Morphing Elastomeric Colloids in Short-Pitch Cholesteric Liquid Crystals. *Phys. Rev. Lett.* **2013**, *110*, 187802.
(22) Gharbi, M. A.; Cavallaro, M. J.; Wu, G.; Beller, D. A.; Kamien, R. D.; Yang, S.; Stebe, K. J. Microbullet Assembly: Interactions of Oriented Dipoles in Confined Nematic Liquid Crystal. *Liq. Cryst.* **2013**, *40*, 1619−27.
(23) Pandey, M. B.; Porenta, T.; Brewer, J.; Burkart, A.; Čopar, S.; Žumer, S.; Smalyukh, I. I. Self-Assembly of Skyrmion-Dressed Chiral Nematic Colloids with Tangential Anchoring. *Phys. Rev. E* **2014**, *89*, 060502.
(24) Silvestre, N. M.; Liu, Q.; Senyuk, B.; Smalyukh, I. I.; Tasinkevych, M. Towards Template-Assisted Assembly of Nematic Colloids. *Phys. Rev. Lett.* **2014**, *112*, 225501.
(25) Smalyukh, I. I. Liquid Crystal Colloids. *Annu. Rev. Condens. Matter Phys.* **2018**, *9*, 207−226.

https://doi.org/10.1021/acs.langmuir.2c00611
Langmuir XXXX, XXX, XXX−XXX

(26) Liu, Q.; Kuzyk, A.; Endo, M.; Smalyukh, I. I. Colloidal Plasmonic DNA-Origami with Photo-Switchable Chirality in Liquid Crystals. *Opt. Lett.* **2019**, *44* (11), 2831−2834.
(27) Wang, N.; Evans, J. S.; Li, C.; Pergamenshchik, V. M.; Smalyukh, I. I.; He, S. Controlled Multistep Self-Assembling of Colloidal Droplets at a Nematic Liquid Crystal-Air Interface. *Phys. Rev. Lett.* **2019**, *123*, 087801.
(28) Sinha, G. P.; Wen, B.; Rosenblatt, C. Large, Continuously Controllable Nematic Pretilt from Vertical Orientation. *Appl. Phys. Lett.* **2001**, *79*, 2543−2545.
(29) Loudet, J. C.; Barois, P.; Auroy, P.; Keller, P.; Richard, H.; Poulin, P. Colloidal Structures from Bulk Demixing in Liquid Crystals. *Langmuir* **2004**, *20*, 11336−11347.
(30) Yada, M.; Yamamoto, J.; Yokoyama, H. Direct Observation of Anisotropic Interparticle Forces in Nematic Colloids with Optical Tweezers. *Phys. Rev. Lett.* **2004**, *92*, 185501.
(31) Ravnik, M.; Škarabot, M.; Žumer, S.; Tkalec, U.; Poberaj, I.; Babič, D.; Osterman, N.; Muševič, I. Entangled Nematic Colloidal Dimers and Wires. *Phys. Rev. Lett.* **2007**, *99*, 247801.
(32) Nych, A. B.; Ognysta, U. M.; Pergamenshchik, V. M.; Lev, B. I.; Nazarenko, V. G.; Muševič, I.; Škarabot, M.; Lavrentovich, O. D. Coexistence of Two Colloidal Crystals at the Nematic-Liquid-Crystal-Air Interface. *Phys. Rev. Lett.* **2007**, *98*, 057801.
(33) Škarabot, M.; Ravnik, M.; Žumer, S.; Tkalec, U.; Poberaj, I.; Babič, D.; Osterman, N.; Muševič, I. Two-dimensional dipolar nematic colloidal crystals. *Phys. Rev. E* **2007**, *76*, 051406.
(34) Škarabot, M.; Ravnik, M.; Žumer, S.; Tkalec, U.; Poberaj, I.; Babič, D.; Muševič, I. Hierarchical self-assembly of nematic colloidal superstructures. *Phys. Rev. E* **2008**, *77*, 061706.
(35) Takahashi, K.; Ichikawa, M.; Kimura, Y. Direct measurement of force between colloidal particles in a nematic liquid crystal. *J. Phys.: Condens. Matter* **2008**, *20*, 075106.
(36) Ognysta, U.; Nych, A.; Nazarenko, V.; Škarabot, M.; Muševič, I. Design of 2D Binary Colloidal Crystals in a Nematic Liquid Crystal. *Langmuir* **2009**, *25*, 12092−12100.
(37) Prathap Chandran, S.; Mondiot, F.; Mondain-Monval, O.; Loudet, J. C. Photonic Control of Surface Anchoring on Solid Colloids Dispersed in Liquid Crystals. *Langmuir* **2011**, *27*, 15185−15198.
(38) Tomar, V.; Roberts, T. F.; Abbott, N. L.; Hernández-Ortiz, J. P.; de Pablo, J. J. Liquid Crystal Mediated Interactions Between Nanoparticles in a Nematic Phase. *Langmuir* **2012**, *28*, 6124−6131.
(39) Eskandari, Z.; Silvestre, N. M.; Telo da Gama, M. M. Bonded Boojum-Colloids in Nematic Liquid Crystals. *Langmuir* **2013**, *29*, 10360−10367.
(40) Cavallaro, M., Jr; Gharbi, M. A.; Beller, D. A.; Čopar, S.; Shi, Z.; Kamien, R. D.; Yang, S.; Baumgart, T.; Stebe, K. J. Ring around the colloid. *Soft Matter* **2013**, *9*, 9099−9102.
(41) Nych, A.; Ognysta, U.; Škarabot, M.; Ravnik, M.; Žumer, S.; Muševič, I. Assembly and control of 3D nematic dipolar colloidal crystals. *Nat. Commun.* **2013**, *4*, 1489.
(42) Zuhail, K. P.; Dhara, S. Temperature dependence of equilibrium separation and lattice parameters of nematic boojum-colloids. *Appl. Phys. Lett.* **2015**, *106*, 211901.
(43) Čopar, S.; Tkalec, U.; Muševič, I.; Žumer, S. Knot theory realizations in nematic colloids. *Proc. Natl. Acad. Sci. U.S.A.* **2015**, *112*, 1675−1680.
(44) Jeridi, H.; Tasinkevych, M.; Othman, T.; Blanc, C. Colloidal Particles in Thin Nematic Wetting Films. *Langmuir* **2016**, *32*, 9097−9107.
(45) Mangal, R.; Nayani, K.; Kim, Y.-K.; Bukusoglu, E.; Córdova-Figueroa, U. M.; Abbott, N. L. Active Janus Particles at Interfaces of Liquid Crystals. *Langmuir* **2017**, *33*, 10917−10926.
(46) Senyuk, B.; Mozaffari, A.; Crust, K.; Zhang, R.; de Pablo, J. J.; Smalyukh, I. I. Transformation between Elastic Dipoles, Quadrupoles, Octupoles, and Hexadecapoles Driven by Surfactant Self-Assembly in Nematic Emulsion. *Sci. Adv.* **2021**, *7*, eabg0377.
(47) Liu, Q.; Cui, Y.; Gardner, D.; Li, X.; He, S.; Smalyukh, I. I. Self-Alignment of Plasmonic Gold Nanorods in Reconfigurable Anisotropic Fluids for Tunable Bulk Metamaterial Applications. *Nano Lett.* **2010**, *10*, 1347.
(48) Jiang, L.; Mundoor, H.; Liu, Q.; Smalyukh, I. I. Electric Switching of Fluorescence Decay in Gold-Silica-Dye Nematic Nanocolloids Mediated by Surface Plasmons. *ACS Nano* **2016**, *10*, 7064−7072.
(49) Park, S.; Mundoor, H.; Fleury, B.; Davidson, P.; van de Lagemaat, J.; Smalyukh, I. I. Liquid Crystalline Order and Electric Switching of Upconversion Luminescence in Colloidal Nanorod Suspensions. *Adv. Opt. Mater.* **2019**, *7*, 1900041.
(50) Ruetschi, M.; Grutter, P.; Funfschilling, J.; Guntherodt, H.-J. Creation of Liquid Crystal Waveguides with Scanning Force Microscopy. *Science* **1994**, *265*, 512−514.
(51) Kim, J.-H.; Yoneya, M.; Yamamoto, J.; Yokoyama, H. Surface alignment bistability of nematic liquid crystals by orientationally frustrated surface patterns. *Appl. Phys. Lett.* **2001**, *78*, 3055.
(52) Ruhwandl, R. W.; Terentjev, E. M. Long-Range Forces and Aggregation of Colloid Particles in a Nematic Liquid Crystal. *Phys. Rev. E* **1997**, *55*, 2958−2961.
(53) Lev, B. I.; Chernyshuk, S. B.; Tomchuk, P. M.; Yokoyama, H. Symmetry Breaking and Interaction of Colloidal Particles in Nematic Liquid Crystals. *Phys. Rev. E* **2002**, *65*, 021709.
(54) Ognysta, U.; Nych, A.; Nazarenko, V.; Muševič, I.; Škarabot, M.; Ravnik, M.; Žumer, S.; Poberaj, I.; Babič, D. 2D Interactions and Binary Crystals of Dipolar and Quadrupolar Nematic Colloids. *Phys. Rev. Lett.* **2008**, *100*, 217803.
(55) Ognysta, U. M.; Nych, A. B.; Uzunova, V. A.; Pergamenschik, V. M.; Nazarenko, V. G.; Škarabot, M.; Muševič, I. Square Colloidal Lattices and Pair Interaction in a Binary System of Quadrupolar Nematic Colloids. *Phys. Rev. E* **2011**, *83*, 041709.
(56) Uzunova, V. A.; Pergamenshchik, V. M. Chiral Dipole Induced by Azimuthal Anchoring on the Surface of a Planar Elastic Quadrupole. *Phys. Rev. E* **2011**, *84*, 031702.
(57) Tovkach, O. M.; Chernyshuk, S. B.; Lev, B. I. Theory of Elastic Interaction between Arbitrary Colloidal Particles in Confined Nematic Liquid Crystals. *Phys. Rev. E* **2012**, *86*, 061703.
(58) Pergamenshchik, V. M. Elastic Multipoles in the Field of the Nematic Director Distortions. *Eur. Phys. J. E* **2014**, *37*, 121.
(59) Lapointe, C.; Mason, T.; Smalyukh, I. I. Shape-Controlled Colloidal Interactions in Nematic Liquid Crystals. *Science* **2009**, *326*, 1083−1086.
(60) Senyuk, B.; Liu, Q.; He, S.; Kamien, R. D.; Kusner, R. B.; Lubensky, T. C.; Smalyukh, I. I. Topological Colloids. *Nature* **2013**, *493*, 200−205.
(61) Senyuk, B.; Liu, Q.; Bililign, E.; Nystrom, P. D.; Smalyukh, I. I. Geometry-Guided Colloidal Interactions and Self-Tiling of Elastic Dipoles Formed by Truncated Pyramid Particles in Liquid Crystals. *Phys. Rev. E* **2015**, *91*, 040501.
(62) Senyuk, B.; Pandey, M. B.; Liu, Q.; Tasinkevych, M.; Smalyukh, I. I. Colloidal Spirals in Nematic Liquid Crystals. *Soft Matter* **2015**, *11*, 8758−8767.
(63) Mundoor, H.; Senyuk, B.; Almansouri, M.; Park, S.; Fleury, B.; Smalyukh, I. I. Electrostatically Controlled Surface Boundary Conditions in Nematic Liquid Crystals and Colloids. *Sci. Adv.* **2019**, *5*, eaax4257.
(64) Razi, M.; Pujala, R. K.; Paladugu, S.; Dhara, S. Interactions of charged microrods in chiral nematic liquid crystals. *Phys. Rev. E* **2021**, *104*, 014706.
(65) Smalyukh, I. I.; Chernyshuk, S.; Lev, B. I.; Nych, A. B.; Ognysta, U.; Nazarenko, V. G.; Lavrentovich, O. D. Ordered Droplet Structures at the Liquid Crystal Surface and Elastic-Capillary Colloidal Interactions. *Phys. Rev. Lett.* **2004**, *93*, 117801.
(66) Senyuk, B.; Puls, O.; Tovkach, O. M.; Chernyshuk, S. B.; Smalyukh, I. I. Hexadecapolar Colloids. *Nat. Commun.* **2016**, *7*, 10659.
(67) Smalyukh, I. I.; Kuzmin, A.; Kachynski, A.; Prasad, P. N.; Lavrentovich, O. D. Optical Trapping of Colloidal Particles and Measurement of the Defect Line Tension and Colloidal Forces in a Thermotropic Nematic Liquid Crystal. *Appl. Phys. Lett.* **2005**, *86*, 021913.

https://doi.org/10.1021/acs.langmuir.2c00611
Langmuir XXXX, XXX, XXX−XXX

(68) Kahn, F. J. Orientation of Liquid Crystals by Surface Coupling Agents. *Appl. Phys. Lett.* **1973**, *22*, 386.
(69) Varney, M. C. M.; Zhang, Q.; Smalyukh, I. I. Stick-Slip Motion of Surface Point Defects Prompted by Magnetically Controlled Colloidal-Particle Dynamics in Nematic Liquid Crystals. *Phys. Rev. E* **2015**, *91*, 052503.
(70) Senyuk, B.; Aplinc, J.; Ravnik, M.; Smalyukh, I. I. High-Order Elastic Multipoles as Colloidal Atoms. *Nat. Commun.* **2019**, *10*, 1825.
(71) Varney, M. C. M.; Zhang, Q.; Senyuk, B.; Smalyukh, I. I. Self-assembly of colloidal particles in deformation landscapes of electrically driven layer undulations in cholesteric liquid crystals. *Phys. Rev. E* **2016**, *94*, 042709.
(72) Kim, J. W.; Larsen, R. J.; Weitz, D. A. Synthesis of Nonspherical Colloidal Particles with Anisotropic Properties. *J. Am. Chem. Soc.* **2006**, *128*, 14374−14377.
(73) Ma, F.; Wang, S.; Smith, L.; Wu, N. Two-Dimensional Assembly of Symmetric Colloidal Dimers Under Electric Fields. *Adv. Funct. Mater.* **2012**, *22*, 4334−4343.
(74) Wang, S.; Ma, F.; Zhao, H.; Wu, N. Bulk Synthesis of Metal-Organic Hybrid Dimers and Their Propulsion Under Electric Fields. *ACS Appl. Mater. Interfaces* **2014**, *6*, 4560−4569.
(75) Senyuk, B.; Varney, M. C. M.; Lopez, J. A.; Wang, S.; Wu, N.; Smalyukh, I. I. Magnetically responsive gourd-shaped colloidal particles in cholesteric liquid crystals. *Soft Matter* **2014**, *10*, 6014−6023.
(76) Zhou, Y.; Senyuk, B.; Zhang, R.; Smalyukh, I. I.; de Pablo, J. J. Degenerate Conic Anchoring and Colloidal Elastic Dipole-Hexadecapole Transformations. *Nat. Commun.* **2019**, *10*, 1000.
(77) Ramdane, O. O.; Auroy, P.; Forget, S.; Raspaud, E.; Martinot-Lagarde, P.; Dozov, I. Memory-Free Conic Anchoring of Liquid Crystals on a Solid Substrate. *Phys. Rev. Lett.* **2000**, *84*, 3871−3874.
(78) Mundoor, H.; Senyuk, B.; Smalyukh, I. I. Triclinic Nematic Colloidal Crystals from Competing Elastic and Electrostatic Interactions. *Science* **2016**, *352*, 69−73.
(79) Mundoor, H.; Park, S.; Senyuk, B.; Wensink, H. H.; Smalyukh, I. I. Hybrid Molecular-Colloidal Liquid Crystals. *Science* **2018**, *360*, 768−771.
(80) Everts, J. C.; Senyuk, B.; Mundoor, H.; Ravnik, M.; Smalyukh, I. I. Anisotropic Electrostatic Screening of Charged Colloids in Nematic Solvents. *Sci. Adv.* **2021**, *7*, eabd0662.
(81) Mundoor, H.; Wu, J.-S.; Wensink, H. H.; Smalyukh, I. I. Thermally Reconfigurable Monoclinic Nematic Colloidal Fluids. *Nature* **2021**, *590*, 268−274.
(82) Senyuk, B.; Mundoor, H.; Smalyukh, I. I.; Wensink, H. H. Nematoelasticity of Hybrid Molecular-Colloidal Liquid Crystals. *Phys. Rev. E* **2021**, *104*, 014703.
(83) Wang, F.; Han, Y.; Lim, C. S.; Lu, Y.; Wang, J.; Xu, J.; Chen, H.; Zhang, C.; Hong, M.; Liu, X. Simultaneous Phase and Size Control of Upconversion Nanocrystals Through Lanthanide Doping. *Nature* **2010**, *463*, 1061−1065.
(84) Mundoor, H.; Smalyukh, I. I. Mesostructured Composite Materials with Electrically Tunable Upconverting Properties. *Small* **2015**, *11*, 5572−5580.
(85) Bogdan, N.; Vetrone, F.; Ozin, G. A.; Capobianco, J. A. Synthesis of Ligand-Free Colloidally Stable Water Dispersible Brightly Luminescent Lanthanide-Doped Upconverting Nanoparticles. *Nano Lett.* **2011**, *11*, 835−840.
(86) Burylov, S. V.; Raikher, Yu. L. On the orientation of an anisometric particle suspended in a bulk uniform nematic. *Phys. Lett. A* **1990**, *149*, 279−283.
(87) Burylov, S. V.; Raikher, Y. L. Orientation of a solid particle embedded in a monodomain nematic liquid crystal. *Phys. Rev. E* **1994**, *50*, 358−367.
(88) Lapointe, C. P.; Hopkins, S.; Mason, T. G.; Smalyukh, I. I. Electrically-Driven Multi-axis Rotational Dynamics of Colloidal Platelets in Nematic Liquid Crystals. *Phys. Rev. Lett.* **2010**, *105*, 178301.
(89) Lapointe, C. P.; Mason, T. G.; Smalyukh, I. I. Towards Total Photonic Control of Complex-Shaped Colloids by Vortex Beams. *Opt. Express* **2011**, *19*, 18182.
(90) Baldacchini, T. *Three-Dimensional Microfabrication Using Two-Photon Polymerization*, 2nd ed.; Elsevier, 2019.
(91) Cumpston, B. H.; Ananthavel, S. P.; Barlow, S.; Dyer, D. L.; Ehrlich, J. E.; Erskine, L. L.; Heikal, A. A.; Kuebler, S. M.; Lee, I. -Y. S.; McCord-Maughon, D.; Qin, J.; Röckel, H.; Rumi, M.; Wu, X.; Marder, S. R.; Perry, J. W. Two-Photon Polymerization Initiators for Three-Dimensional Optical Data Storage and Microfabrication. *Nature* **1999**, *398*, 51−54.
(92) Liu, Q.; Senyuk, B.; Tasinkevych, M.; Smalyukh, I. I. Nematic Liquid Crystal Boojums with Handles on Colloidal Handlebodies. *Proc. Natl. Acad. Sci. U.S.A.* **2013**, *110*, 9231.
(93) Senyuk, B.; Liu, Q.; Nystrom, P. D.; Smalyukh, I. I. Repulsion-Attraction Switching of Nematic Colloids Formed by Liquid Crystal Dispersions of Polygonal Prisms. *Soft Matter* **2017**, *13*, 7398−7405.
(94) Wang, Y. F.; Wang, Y.; Breed, D. R.; Manoharan, V. N.; Feng, L.; Hollingsworth, A. D.; Weck, M.; Pine, D. J. Colloids with Valence and Specific Directional Bonding. *Nature* **2012**, *491*, 51−55.
(95) Martinez, A.; Lee, T.; Asavei, Th.; Rubinsztein-Dunlop, H.; Smalyukh, I. I. Three-Dimensional Complex-Shaped Photopolymerized Microparticles at Liquid Crystal Interfaces. *Soft Matter* **2012**, *8*, 2432−2437.
(96) Martinez, A.; Ravnik, M.; Lucero, B.; Visvanathan, R.; Žumer, S.; Smalyukh, I. I. Mutually Tangled Colloidal Knots and Induced Defect Loops in Nematic Fields. *Nat. Mater.* **2014**, *13*, 258.
(97) Martinez, A.; Hermosillo, L.; Tasinkevych, M.; Smalyukh, I. I. Linked Topological Colloids in a Nematic Host. *Proc. Natl. Acad. Sci. U.S.A.* **2015**, *112*, 4546−4551.
(98) Yuan, Y.; Martinez, A.; Senyuk, B.; Tasinkevych, M.; Smalyukh, I. I. Chiral Liquid Crystal Colloids. *Nat. Mater.* **2018**, *17*, 71−79.
(99) Hashemi, S. M.; Jagodič, U.; Mozaffari, M. R.; Ejtehadi, M. R.; Muševič, I.; Ravnik, M. Fractal Nematic Colloids. *Nat. Commun.* **2017**, *8*, 14026.
(100) Livingston, C. *Knot Theory*; The Mathematical Association of America, Indiana University: Bloomington, 1993.
(101) Kauffman, L. H. *Knots and Physics*, 3rd ed.; World Scientific, 2000.
(102) Bonaccorso, F.; Sun, Z.; Hasan, T.; Ferrari, A. C. Graphene Photonics and Optoelectronics. *Nat. Photonics* **2010**, *4*, 611−622.
(103) Senyuk, B.; Behabtu, N.; Martinez, A.; Lee, T.; Tsentalovich, D. E.; Ceriotti, G.; Tour, J. M.; Pasquali, M.; Smalyukh, I. I. Three-Dimensional Patterning of Solid Microstructures Through Laser Reduction of Colloidal Graphene Oxide in Liquid-Crystalline Dispersions. *Nat. Commun.* **2015**, *6*, 7157.
(104) Marcano, D. C.; Kosynkin, D. V.; Berlin, J. M.; Sinitskii, A.; Sun, Z.; Slesarev, A.; Alemany, L. B.; Lu, W.; Tour, J. M. Improved Synthesis of Graphene Oxide. *ACS Nano* **2010**, *4*, 4806−4814.
(105) Senyuk, B.; Behabtu, N.; Pacheco, B. G.; Lee, T.; Ceriotti, G.; Tour, J. M.; Pasquali, M.; Smalyukh, I. I. Nonlinear Photoluminescence Imaging of Isotropic and Liquid Crystalline Dispersions of Graphene Oxide. *ACS Nano* **2012**, *6*, 8060−8066.
(106) Martinez, A.; Mireles, H. C.; Smalyukh, I. I. Large-Area Optoelastic Manipulation of Colloidal Particles in Liquid Crystals Using Photoresponsive Molecular Surface Monolayers. *Proc. Natl. Acad. Sci. U.S.A.* **2011**, *108*, 20891−20896.
(107) Yuan, Y.; Abuhaimed, G. N.; Liu, Q.; Smalyukh, I. I. Self-Assembled Nematic Colloidal Motors Powered by Light. *Nat. Commun.* **2018**, *9*, 5040.
(108) Ma, L.; Liu, C.; Wu, S.; Chen, P.; Chen, Q.; Qian, J.; Ge, S.; Wu, Y.; Hu, W.; Lu, Y. Programmable Self-Propelling Actuators Enabled by a Dynamic Helical Medium. *Sci. Adv.* **2021**, *7*, eabh3505.
(109) Eelkema, R.; Pollard, M. M.; Vicario, J.; Katsonis, N.; Ramon, B. S.; Bastiaansen, C. W.; Broer, D. J.; Feringa, B. L. Nanomotor Rotates Microscale Objects. *Nature* **2006**, *440*, 163.
(110) Straube, A. V.; Pagès, J. M.; Ortiz-Ambriz, A.; Tierno, P.; Ignés-Mullol, J.; Sagués, F. Assembly and Transport of Nematic Colloidal Swarms above Photo-Patterned Defects and Surfaces. *New J. Phys.* **2018**, *20*, 075006.

https://doi.org/10.1021/acs.langmuir.2c00611
Langmuir XXXX, XXX, XXX−XXX

(111) Sahu, D. K.; Dhara, S. Electrophoresis of metal-dielectric Janus particles with dipolar director symmetry in nematic liquid crystals. *Soft Matter* **2022**, *18*, 1819−1824.
(112) Sahu, D. K.; Kole, S.; Ramaswamy, S.; Dhara, S. Omnidirectional transport and navigation of Janus particles through a nematic liquid crystal film. *Phys. Rev. Res.* **2020**, *2*, 032009.
(113) Eremin, A.; Hirankittiwong, P.; Chattham, N.; Nádasi, H.; Stannarius, R.; Limtrakul, J.; Haba, O.; Yonetake, K.; Takezoe, H. Optically Driven Translational and Rotational Motions of Microrod Particles in a Nematic Liquid Crystal. *Proc. Natl. Acad. Sci. U.S.A.* **2015**, *112*, 1716−1720.
(114) Kuwahara, Y.; Oda, T.; Kim, S.; Ogata, T.; Kurihara, S. Photo-Responsive Traveling of Small-Particles Modified with Azobenzene Groups as Molecular Motors in a Liquid Crystal. *Mater. Lett.* **2016**, *181*, 257−260.
(115) Yuan, Y.; Liu, Q.; Senyuk, B.; Smalyukh, I. I. Elastic Colloidal Monopoles and Reconfigurable Self-Assembly in Liquid Crystals. *Nature* **2019**, *570*, 214−218.
(116) Yamamoto, T.; Tabe, Y.; Yokoyama, H. Manipulation of Defect Structures and Colloidal Chains in Liquid Crystals by Means of Photochemical Reactions of Azobenzene Compounds. *Mol. Cryst. Liq. Cryst.* **2009**, *498*, 1−10.
(117) Yamamoto, T.; Tabe, Y.; Yokoyama, H. Photochemical Manipulation of Colloidal Structures in Liquid-Crystal Colloids. *Proc. SPIE* **2007**, *6587*, 658707.
(118) Yamamoto, T.; Yamamoto, J.; Lev, B. I.; Yokoyama, H. Light-Induced Assembly of Tailored Droplet Arrays in Nematic Emulsions. *Appl. Phys. Lett.* **2002**, *81*, 2187.
(119) Yamamoto, T.; Yamamoto, J.; Lev, B. I.; Yokoyama, H. Photochemical Manipulation of Glycerol Droplets in Nematic Liquid Crystals. *Mol. Cryst. Liq. Cryst.* **2004**, *409*, 111−117.
(120) Yamamoto, T.; Yoshida, M. Photoinduced Directional Motions of Microparticles at Air−Liquid-Crystal Interfaces of Azobenzene-Doped Liquid-Crystal Films with Homeotropic or Homogeneous Alignment Structures. *Appl. Phys. Express* **2012**, *5*, 101701.
(121) Yamamoto, T.; Yoshida, M. Photochemical Manipulation of Microparticles on Azobenzene-Doped Liquid-Crystal Films with Homogeneous or Homeotropic Alignment Structures. *Proc. SPIE* **2012**, *8475*, 847505.
(122) Kausar, A.; Nagano, H.; Ogata, T.; Nonaka, T.; Kurihara, S. Photocontrolled Translational Motion of a Microscale Solid Object on Azobenzene-Doped Liquid-Crystalline Films. *Angew. Chem., Int. Ed.* **2009**, *48*, 2144−2147.
(123) Yamamoto, T.; Tabe, Y.; Yokoyama, H. Photochemical Transformation of Topological Defects Formed around Colloidal Droplets Dispersed in Azobenzene-Containing Liquid Crystals. *Colloids Surf. A: Physicochem. Eng. Asp.* **2009**, *334*, 155−159.
(124) Yi, Y.; Farrow, M.; Korblova, E.; Walba, D. M.; Furtak, T. E. High-Sensitivity Aminoazaobenzene Chemisorbed Monolayers for Photoalignment of Liquid Crystals. *Langmuir* **2009**, *25*, 997−1003.
(125) Senyuk, B.; Adufu, R. E.; Smalyukh, I. I. Electrically Powered Locomotion of Dual-Nature Colloid-Hedgehog and Colloid-Umbilic Topological and Elastic Dipoles in Liquid Crystals. *Langmuir* **2022**, *38*, 689−697.
(126) Yuan, Y.; Keller, P.; Smalyukh, I. I. Elastomeric Nematic Colloids, Colloidal Crystals and Microstructures with Complex Topology. *Soft Matter* **2021**, *17*, 3037−3046.
(127) Fleury, B.; Senyuk, B.; Tasinkevych, M.; Smalyukh, I. I. Interplay of Electrostatic Dipoles and Monopoles with Elastic Interactions in Nematic Liquid Crystal Nanocolloids. *Nano Lett.* **2020**, *20*, 7835−7843.
(128) Yuan, Y.; Tasinkevych, M.; Smalyukh, I. I. Colloidal Interactions and Unusual Crystallization Versus De-Mixing of Elastic Multipoles Formed by Gold Mesoflowers. *Nat. Commun.* **2020**, *11*, 188.
(129) Park, S.; Mundoor, H.; Fleury, B.; Davidson, P.; van de Lagemaat, J.; Smalyukh, I. I. Liquid Crystalline Order and Electric Switching of Upconversion Luminescence in Colloidal Nanorod Suspensions. *Adv. Opt. Mater.* **2019**, *7*, 1900041.
(130) Park, S.; Liu, Q.; Smalyukh, I. I. Colloidal Surfaces with Boundaries, Apex Boojums, and Nested Elastic Self-Assembly of Nematic Colloids. *Phys. Rev. Lett.* **2016**, *117*, 277801.
(131) Trivedi, R. P.; Tasinkevych, M.; Smalyukh, I. I. Nonsingular Defects and Self-Assembly of Colloidal Particles in Cholesteric Liquid Crystals. *Phys. Rev. E* **2016**, *94*, 062703.
(132) Senyuk, B.; Liu, Q.; Yuan, Y.; Smalyukh, I. I. Edge Pinning and Transformation of Defect Lines Induced by Faceted Colloidal Rings in Nematic Liquid Crystals. *Phys. Rev. E* **2016**, *93*, 062704.
(133) Pandey, M. B.; Ackerman, P. J.; Burkart, A.; Porenta, T.; Žumer, S.; Smalyukh, I. I. Topology and Self-Assembly of Defect-Colloidal Superstructure in Confined Chiral Nematic Liquid Crystals. *Phys. Rev. E* **2015**, *91*, 012501.
(134) Porenta, T.; Čopar, S.; Ackerman, P. J.; Pandey, M. B.; Varney, M. C. M.; Smalyukh, I. I.; Žumer, S. Topological Switching and Orbiting Dynamics of Colloidal Spheres Dressed with Chiral Nematic Solitons. *Sci. Rep.* **2015**, *4*, 7337.
(135) Varney, M. C. M.; Zhang, Q.; Tasinkevych, M.; Silvestre, N. M.; Bertness, K. A.; Smalyukh, I. I. Periodic Dynamics, Localization Metastability, and Elastic Interaction of Colloidal Particles with Confining Surfaces and Helicoidal Structure of Cholesteric Liquid Crystals. *Phys. Rev. E* **2014**, *90*, 062502.
(136) Sun, Y.; Evans, J. S.; Lee, T.; Senyuk, B.; Keller, P.; He, S.; Smalyukh, I. I. Optical Manipulation of Birefringent Shape-Morphing Colloidal Microparticles Made from Liquid Crystal Elastomers Doped with Gold Nanospheres. *Appl. Phys. Lett.* **2012**, *100*, 241901.
(137) Trivedi, R. P.; Klevets, I. I.; Senyuk, B.; Lee, T.; Smalyukh, I. I. Reconfigurable Interactions and Three-Dimensional Patterning of Colloidal Particles and Defects in Lamellar Soft Media. *Proc. Natl. Acad. Sci. U.S.A.* **2012**, *109*, 4744.
(138) Senyuk, B.; Evans, J. S.; Ackerman, P.; Lee, T.; Manna, P.; Vigderman, L.; Zubarev, E. R.; van de Lagemaat, J.; Smalyukh, I. I. Shape-Dependent Oriented Trapping and Scaffolding of Plasmonic Nanoparticles by Topological Defects for Self-Assembly of Colloidal Dimers in Liquid Crystals. *Nano Lett.* **2012**, *12*, 955−963.
(139) Muševič, I.; Škarabot, M.; Tkalec, U.; Ravnik, M.; Žumer, S. Two-Dimensional Nematic Colloidal Crystals Self-Assembled by Topological Defects. *Science* **2006**, *313*, 954−58.
(140) Evans, J. S.; Beier, C.; Smalyukh, I. I. Alignment of High-Aspect Ratio Colloidal Gold Nanoplatelets in Nematic Liquid Crsytals. *J. Appl. Phys.* **2011**, *110*, 033535.
(141) Fukuda, J.; Stark, H.; Yoneya, M.; Yokoyama, H. Interaction between Two Spherical Particles in a Nematic Liquid Crystal. *Phys. Rev. E* **2004**, *69*, 041706.
(142) Senyuk, B.; Glugla, D.; Smalyukh, I. I. Rotational and Translational Diffusion of Anisotropic Gold Nanoparticles in Liquid Crystals Controlled by Varying Surface Anchoring. *Phys. Rev. E* **2013**, *88*, 062507.
(143) Ackerman, P. J.; Smalyukh, I. I. Static Three-Dimensional Topological Solitons in Fluid Chiral Ferromagnets and Colloids. *Nat. Mater.* **2017**, *16*, 426−432.
(144) Liu, Q.; Ackerman, P. J.; Lubensky, T. C.; Smalyukh, I. I. Biaxial Ferromagnetic Liquid Crystal Colloids. *Proc. Natl. Acad. Sci. U.S.A.* **2016**, *113*, 10479−10484.
(145) Trivedi, R. P.; Engström, D.; Smalyukh, I. I. Optical Manipulation of Colloids and Defect Structures in Anisotropic Liquid Crystal Fluids. *J. Opt.* **2011**, *13*, 044001.
(146) Ryzhkova, A. V.; Muševič, I. Particle Size Effects on Nanocolloidal Interactions in Nematic Liquid Crystals. *Phys. Rev. E* **2013**, *87*, 032501.
(147) Škarabot, M.; Ravnik, M.; Žumer, S.; Tkalec, U.; Poberaj, I.; Babič, D.; Osterman, N.; Muševič, I. Two-Dimensional Dipolar Nematic Colloidal Crystals. *Phys. Rev. E* **2007**, *76*, 051406.
(148) Zhang, Q.; Ackerman, P. J.; Liu, Q.; Smalyukh, I. I. Ferromagnetic Switching of Knotted Vector Fields in Liquid Crystal Colloids. *Appl. Phys. Lett.* **2015**, *115*, 097802.
(149) Kishita, T.; Kondo, N.; Takahashi, K.; Ichikawa, M.; Fukuda, J.; Kimura, Y. Interparticle Force in Nematic Colloids: Comparison between Experiment and Theory. *Phys. Rev. E* **2011**, *84*, 021704.

https://doi.org/10.1021/acs.langmuir.2c00611
Langmuir XXXX, XXX, XXX−XXX

(150) Muševič, I. *Liquid Crystal Colloids*; Springer, 2017.
(151) Sahu, D. K.; Dhara, S. Measuring electric-field-induced dipole moments of metal-dielectric Janus particles in a nematic liquid crystal. *Phys. Rev. Appl.* **2020**, *14*, 034004.
(152) Sahu, D. K.; Dhara, S. Electric field driven controllable motility of metal-dielectric Janus particles with boojum defects in thin films of a nematic liquid crystal. *Phys. Fluids* **2021**, *33*, 087106.

https://doi.org/10.1021/acs.langmuir.2c00611
Langmuir XXXX, XXX, XXX−XXX